Feedback in the brainstem: An excitatory disynaptic pathway for control of whisking

David W. Matthews[1,2], **Martin Deschênes**[3], **Takahiro Furuta**[4], **Jeffrey D. Moore**[1,2], **Fan Wang**[5], **Harvey J. Karten**[1,6,*], and **David Kleinfeld**[1,2,7,*]

[1]Graduate Program in Neuroscience, University of California, San Diego, La Jolla, CA 92093 USA

[2]Department of Physics, University of California, San Diego, La Jolla, CA 92093 USA

[3]Centre de Recherche Université Laval Robert-Giffard, Québec City, Quebec G1J 2R3, Canada

[4]Department of Morphological Brain Science, Graduate School of Medicine, Kyoto University, Kyoto 606-8501, Japan

[5]Department of Cell Biology, Duke University Medical Center, Durham, NC 27710, USA

[6]Department of Neuroscience, University of California, San Diego, School of Medicine, La Jolla, CA 92093 USA.

[7]Section of Neurobiology, University of California, San Diego, La Jolla, CA 92093 USA

Abstract

Sensorimotor processing relies on hierarchical neuronal circuits to mediate sensory-driven behaviors. In the mouse vibrissa system, trigeminal brainstem circuits are thought to mediate the first stage of vibrissa scanning control via sensory feedback that provides reflexive protraction in response to stimulation. However, these circuits are not well defined. Here, we describe a complete disynaptic sensory receptor-to-muscle circuit for positive feedback in vibrissa movement. We identified a novel region of trigeminal brainstem, *spinal trigeminal nucleus pars muralis*, that contains a class of vGluT2+ excitatory projection neurons involved in vibrissa motor control. Complementary single- and duallabeling with traditional and virus tracers demonstrate that these neurons both receive primary inputs from vibrissa sensory afferent fibers and send monosynaptic connections to facial nucleus motoneurons that directly innervate vibrissa musculature. These anatomical results suggest a general role of disynaptic architecture in fast positive feedback for motor output driving active sensation.

Indexing terms

---

[*]Corresponding authors are David Kleinfeld (dk@physics.ucsd.edu) and Harvey J. Karten (hjkarten@ucsd.edu).

CONFLICT OF INTEREST STATEMENT
We have no conflicts of interest.

Behavior is the purposeful and reactive motor output of an animal in response to sensory input (Powers 1973, Skinner 1938). In all vertebrates, motor control for behavior results from the coordinated activity of parallel, hierarchical neuronal circuits. Selective pressure for fast, context-relevant movement presumably minimizes the computational complexity, in terms of the number of synaptic relays, between sensors and effectors. For example, the spinal stretch reflex involves a monosynaptic, excitatory circuit from Ia afferent fibers to alpha motoneurons for positive feedback and a disynaptic, inhibitory circuit via 1a interneurons to antagonist muscles (Burke 2004, Jankowska 1992, Kiehn 2006). For behaviors that involve more than one motor primitive, neuronal feedback loops in the spinal cord and brainstem underlie active sensation and thus guide motor output to enhance behaviorally relevant sensory inputs (Gibson 1962, Kleinfeld et al 2006, Schroeder et al 2010). Physiological experiments suggest that disynaptic excitatory circuits are necessary for a range of low-level behaviors. These include grasping (Bui et al 2013) and locomotion (Angel et al 2005) in spinal cord and the vestibulo-ocular and optokinetic reflexes (Graf et al 2002), vibrissa motion (Nguyen & Kleinfeld 2005), and modulation of respiration (Kirkwood & Sears 1982) in the brainstem. Yet, with the exception of the recently described grasp response (Bui et al 2013), definitive anatomical evidence for such disynaptic brainstem circuits, which underlie local reflexes that shape and coordinate orofacial behaviors, is absent (Burke 2004, Jankowska 1992).

We focus on the trigemino-facial brainstem of mouse, which mediates active sensation in vibrissa sensorimotor behavior (Kleinfeld et al 1999, Nelson & MacIver 2006), to delineate the entire anatomy of a circuit from sensor to effector. Neurons in the trigeminal ganglion (Vg) receive sensory signals from afferent neurons that innervate vibrissae and cutaneous skin on the face (Rice 1993, Rice et al 1997), and terminate throughout the trigeminal nuclear complex (Arvidsson 1982, Astrom 1953, Cajal 1905, Kerr 1963, Marfurt 1981), which is composed of four heterogeneous nuclei situated in the pons, medulla, and rostral spinal cord (Olszewski 1950). The trigeminal complex contains both excitatory and inhibitory interneurons (Avendano et al 2005, Furuta et al 2006, Furuta et al 2008, Li et al 1997) that project within and among the nuclei (Bellavance et al 2010, Jacquin et al 1989a, Jacquin et al 1989b), as well as directly or indirectly to lateral facial nucleus (VIIm), which controls vibrissa musculature (Courville 1966, Klein & Rhoades 1985, Komiyama et al 1984) (Fig. 1A). However, the origin, extent, and terminal zones of trigeminal afferent inputs and trigeminofacial projections are disputed (Erzurumlu & Killackey 1979, Hattox et al 2002, Holstege et al 1986, Isokawa-Akesson & Komisaruk 1987, Panneton & Martin 1983, Pellegrini et al 1995, Takeuchi et al 1979, Travers & Norgen 1983, van Ham & Yeo 1996). In particular, initial studies of trigeminofacial connectivity used large lesions (Erzurumlu & Killackey 1979) or injections of large volumes of anterograde tracer (Hattox et al 2002), both of which are likely to include neurons outside of the targeted nucleus of interest. More recent behavioral and physiological preparations evaluating the projections of trigeminal nucleus to VIIm (Pinganaud et al 1999) suggest a net excitatory circuit, possibly to improve sensory acuity during whisking (Nguyen & Kleinfeld 2005, Sachdev et al 2003). Here, we aimed to identify the shortest feedback pathway in the trigeminofacial system in order to elucidate general circuit principles of low-level sensorimotor feedback in the brainstem.

MATERIALS AND METHODS

Animals

Seventy-five animals were used across all experiments. Sixty-three were C57Bl/6 adult male mice (age 8 to 9 weeks). Four were postnatal mice that produces rabies glycoprotein in cholineric neurons, for which we crossed Chat-Cre transgenic mice (B6;129S6-*Chat*$^{tm2(cre)Lowl}$/J) (no. 006410; Jackson Laboratories) with floxed-stop-glycoprotein transgenic mice (B6.129P2-*Gt(ROSA)26Sor*$^{tm1(CAG-RABVgp4,-TVA)Arenk}$/J) (no. 024708; Jackson Laboratories); the final animals are denoted RΦGT mice (Takatoh et al 2013). Two animals (age 8 weeks) were BAC transgenic mice that expressed enhanced green fluorescent protein (EGFP) via the promoter for the vesicular Gaba transporter (VGAT) (B6.Cg-Tg(Slc32a1-COP4*H134R/EYFP)8Gfng/J) (no. 014548; Jackson Laboratories) (Zhao et al 2011). Two animals (age 8 weeks) were BAC transgenic mice that expressed EGFP via the promoter for the glycine transporter (GlyT2) (slc6a5-EGFP) (Zeilhofer et al 2005). Two animals (age 8 weeks) were knockin transgenic mice that expressed EGFP via the promoter for glutamic acid decarboxylase (GAD67) (Tamamaki et al 2003). Lastly, two animals (age 8 weeks) were knockin transgenic mice that expressed EGFP via the promoter for GAD67 apparently only in cells that, in many brain areas but still unproven for brainstem, also express somatostain (FVB-Tg(GadGFP)45704Swn/J) (no. 003718, Jackson Laboratories) and are referred to as GFP-expressing inhibitory neuron (GIN) mice (Oliva Jr et al 2000). Where necessary, animals were anesthetized with either inhalation isoflurane (0.5 – 2.5 % in O_2) for experiments involving no VIIm output, or ketamine and xylazine (0.13 and 0.01 mg/g body weight, respectively). Body temperature was always maintained at 37°C. Animal care and treatment conformed to the National Institutes of Health Guidelines and were approved by the Institutional Animal Care and Use at University of California, San Diego. The investigator performing experiments was properly vaccinated against rabies, and experiments were performed in a Biosafety 2 laboratory.

Stereotaxic injections of tracers and viruses

For peripheral sensory nerve labeling experiments, ~ 1.0 – 2.0 μL of 1 % (w/v) cholera toxin subunit B (CTb, no. 103B; List Laboratories) (Angelucci et al 1996) was injected subcutaneously and unilaterally on the left hemi-section of the face into one of maxillary, mandibular, or ophthalmic nerve terminal branching zones of trigeminal ganglion (Vg) afferent neurons. Injections were made with a 10 μL Hamilton syringe (Hamilton Company) coupled to tubing and a 30-gauge injection needle. For full trigeminal ganglion labeling, the mouse was positioned in a stereotaxic instrument (M900; Kopf), and a 2 mm by 2 mm craniotomy was centered at 1.5 mm rostral to bregma and 1.7 mm left of the midline. In some cases (8 of 15), vibrissa-responsive neurons in Vg were located by manual mechanical stimulation of the ipsilateral vibrissae while extracellular recording in Vg with a thin tip diameter (~ 10 μm) quartz pipette filled with 0.5 M NaCl, amplified (Axoclamp 900A; Molecular Devices), and observed on an oscilloscope (Tektronix TDS 224) and audio speaker. Vg vibrissa-responsive neuron locations in the maxillary branch were consistent relative to stereotaxic coordinates, precluding the need to record in all animals. A thin quartz injection pipette (0.6 mm ID, 1.0 mm OD, pulled to ~ 20 μm tip on P-2000, Sutter Instrument) was advanced to 5.7 – 6.0 mm below the surface, or the precise location of

maximal vibrissa responses, with a micrometer-resolution manipulator (MPC-200, Sutter Instrument), and ~ 80 – 400 nL of 0.5 or 1 % (w/v) CTb was injected by pressure using a custom circuit triggered by a pulse generator (Grass S48 stimulator). Animals were allowed to survive for 3 – 10 d to maximize labeling of afferent projections in brainstem.

For disynaptic motor projection labeling experiments with virus, a 10 μL Hamilton syringe was passed through an ~ 2 – 3 mm incision dorsal to the A-row vibrissae of the left face, and advanced into the mystacial pad musculature. Several focal injections of the 152 Bartha strain of Pseudorabies virus (PRV) (titer: 1×10^9) were made along the dorsoventral axis of the pad with a total injected volume of 5.0 – 7.0 μL. After suturing the incision, the virus incubated in the live animal for 48 – 72 h, to determine optimal transsynaptic labeling protocol.

For identifying facial nucleus (VIIm) motoneurons projecting to vibrissae musculature, a tungsten single channel electrode (0.5 MΩ, WE30030.5A10; MicroProbes) was advanced just caudal to the transverse sinus, through a cranial window centered 5.5 mm caudal to bregma and 1.5 mm left of the midline. To improve access to the rostral portion of lateral VIIm without damaging the sinus, the head was pitched such that the bregma-lambda horizontal of the skull was 6° below parallel. A microstimulation protocol of 100 – 200 μs pulses at 10 ms intervals for 100 ms, over a range of 500 nA to 20 μA, was used to identify exclusively or primarily vibrissa-controlling motoneurons (Isolated Pulse Stimulator 2100; A-M Systems). When sufficient vibrissa movement was elicited from minimal stimulation intensity, generally < 2 μA, at 4.8 – 5.2 mm below brain surface, the stimulation electrode was replaced with a quartz injection electrode with 6–25 μm tip diameter, depending on the reagent. For FluoroGold (2 % (w/v) in 0.1 M cacodylic acid; Sigma) injections, the reagent was iontophoresed using positive current pulses from an Axoclamp 900A amplifier of 150 – 400 nA at 2 Hz half duty cycle for 20 min. The animals were allowed to recover for 2 – 3 d. For rabies virus injections, glycoprotein-deleted rabies (G-RV; pSAD-dG-GFP-M0; titer: 4.1×10^9 units/mL) was pressure-injected over 5 min, followed by 5 min delay before removing the pipette. In both cases, we used a separate pipette for stimulation and injection to avoid, in the case of FluoroGold, pre-injection leakage of the charged tracer, and, in the case of virus, possible spread to local regions. The ChAT-mediated rabies injection and molecular strategy has been described elsewhere (Takatoh et al 2013).

Perfusion, immunohistochemistry, and in situ hybridization

Mice were deeply anesthetized with inhalation isoflurane (3 – 4 % in O_2) followed by intraperitoneal injection of 100 – 200 μL pentobarbital (Fatal Plus), transcardially perfused with phosphate-buffered saline followed by 4 % (w/v) paraformaldehyde in phosphate-buffered saline (PBS) (P3813; Sigma) pH 7.4. After removal from the skull and at least three hours of 4 % (w/v) PFA exposure, the brain, trigeminal ganglion and nerve, and facial skin were each cryoprotected in 30 % (w/v) sucrose in 0.1 M PBS, and sectioned on a freezing microtome. Brain and upper cervical spinal cord were serially sectioned at 30 μm (CTb and some light microscopy tissue) or 60 μm (all other tissue) in one of three standard stereotaxic planes (sagittal, coronal, and horizontal), though data is shown from sagittal and horizontal sections only. For dark product reactions of CTb cases, sequential sections were treated with

Nissl stain (Cresyl violet acetate, C-5042; sigma), Giemsa (Original Azure Stain, WVR 15204-144), and Goat anti-cholera toxin primary antibody (1:12,000, no. 703; List laboratories; RRID: AB_10013220) followed by biotinylated rabbit anti-goat IgG (1:200, no. BA-5000; Vector Company; RRID: AB_2336126) and 0.025 mg/mL DAB solution (D-5637; Sigma). Face and ganglion sections, where treated, were prepared similarly. Sections were mounted, dehydrated in ascending alcohols, delipidized in xylenes, and cover-slipped with Cytoseal 60 (NC952739; Fisher Scientific). For all other dark reaction product experiments, sequential sections were incubated in immuno-blocking buffer (2 % (v/v) normal horse serum and 0.25 % (v/v) Triton-X in PBS) for 12 – 18 h, treated with the relevant primary antibody for pseudorabies (1:1000, Ab3534; Abcam; RRID: AB_303884), GFP (1:1000, NB600-308; Novus Biologicals; RRID: AB_10003058) or FluoroGold (1:4000, AB153; Millipore; RRID: AB_90738), washed with 0.1 M PBS, incubated in cytochrome C (300 μg/mL) and 3,3'-diaminobenzidine (DAB) (500 μg/mL) for 30 min to 2 h at 37°C, washed with 0.1 M PBS, incubated in ABC Elite kit (Vector Labs, CA) for 3 h, revealed with SG ImmPACT kit (Vector), mounted, dehydrated, delipidized, and cover-slipped (Permount, Electron Microscopy Sciences).

For fluorescence experiments, sections were sliced at 30 μm, mounted on gelatin-coated slides, air-dried, rinsed with 1 M PBS, incubated for at least 20 min at room temperature in immuno-blocking buffer, then incubated 12 – 18 h in the same blocking buffer with a primary antibody to the virus or tracer as listed above. Intrinsic GFP fluorescence of rabies-GFP was sufficiently strong to preclude antibody labeling. After rinsing with 0.1 M PBS, sections were incubated for 2 h with appropriate secondary antibodies (Alexa Fluor 594 donkey anti-goat, 1:200; no. A11058; Life Technologies; RRID: AB_10563390) for 2 h, rinsed, dried, and exposed to a fluorescent Nissl stain, Neurotrace (1:200, N-21479 blue or N-21482 red; Invitrogen), for 40 min, and cover-slipped (Fluoromount G, EMS). As a control for cross-reactivity of the secondary antibody, we tested the Alexa Fluor 594 donkey anti-goat on four sections from wild type mice (1:200) and saw no reaction product.

To retrogradely label facial nucleus-projecting SpVm neurons for *in situ* hybridization, 0.1 μL of 1 % (w/v) Alexa 488-conjugated cholera toxin B subunit (A488-CTB; Invitrogen) dissolved in 0.1 M PBS was pressure injected into lateral facial nucleus of three mice under ketamine/xylazine anesthesia. After a 48 h survival period, the mice were deeply anesthetized and transcardially perfused with 0.1 M PBS, as previously described.

The *in situ* hybridization procedure has been described (Furuta et al 2008). In brief: (*i*) Sections were incubated with 0.3 % (v/v) Triton-X 100 in PBS for 20 minutes; (*ii*) Sections were acetylated in freshly prepared 0.25 % (v/v) acetic anhydride in 0.1 M triethanolamine for 10 minutes; (*iii*) Sections were rinsed in PBS; (*iv*) Sections were hybridized by incubating them for 20 hours at 70° C in a solution containing 1.0 g/mL digoxigenin-labeled sense or antisense RNA probes for either VIAAT, VGluT1, VGluT2, or GAD67 (Table 1), plus 50 % (v/v) formamide, 5-times concentrated sodium citrate buffer, 2 % (v/v) blocking reagent (Roche Diagnostics, Indianapolis), 0.1 % (v/v) N-lauroylsarcosine, and 0.1 % (v/v) sodium dodecyl sulfate; (*v*) Sections were washed twice, for 20 minutes at 70° C, in a solution containing 50 % (w/v) formamide and 0.1 % (v/v) N-lauroylsarcosine in 2-times concentrated sodium citrate buffer; (*vi*) Next they were incubated with 20g/mL RNase A for

30 minutes at 37° C; (*vii*) Sections were washed in 2-times concentrated sodium citrate buffer plus 0.1% N-lauroylsarcosine for 20 minutes at 37° C; (*vii*) Sections were incubated in 0.2-times concentrated sodium citrate buffer plus 0.1% (w/v) N-lauroylsarcosine; (*viii*) Sections were incubated with a mixture of 1:1000 alkaline phosphatase-conjugated sheep anti-digoxigenin antibody Fab fragment (Roche Diagnostics) and 1:1000 anti-FG rabbit antibody (Chemicon, Temecula) in 1 % (v/v) blocking reagent (Roche Diagnostics) diluted in TS7.5 at room temperature for 16 hours; (*x*) Sections were three times in PBS; (*xi*), Sections were incubated with AlexaFluor 488-conjugated goat anti-rabbit IgG (1:100; Invitrogen); and finally (*xii*) the hybridization probe was visualized by reacted sections with the HNPP Fluorescent Detection Set (Roche Diagnostics).

Imaging and digitization

Slides were imaged serially and automatically using a whole-slide imaging scanner (NanoZoomer 2.0-HT, Hamamatsu Photonics, Japan) at 0.453 μm/pixel resolution under a 20× magnification (0.75 NA) objective (Olympus) under illumination from a 200 W mercury lamp. This system uses line scanning of a three-channel time-delay integrated sensor to resolve both fluorescent and brightfield images at ~8 (brightfield) to ~ 25 (fluorescent) min per slide for our tissue. Fluorescent images were collected using a three-filter cube for red, green, and blue spectral separation. All NanoZoomer images were collected at a resolution of 0.5 μm/pixel, and stored in the NanoZoomer variant of the JPEG 2000 file format. Images were evaluated and converted from NDPI format to TIF using ImageScope (Aperio) and leveled and downsampled in Photoshop (Adobe). Confocal imaging was performed on an Olympus FV1000 and a Leica SP5 upright microscope, using 20× air, 100× oil, and 63× magnification glycerol objectives. Images were converted and leveled in Fiji (an open source ImageJ distribution).

For volumetric reconstructions, full-slide images were automatically or manually sectioned according to the position of the tissue slices. Each slice was then traced either manually or semi-automatically, and tracer locations were identified and traced according to intensity of the dark product reaction against the tracer or virus of interest using Neurolucida (MicroBrightField, Inc.). Brain traces were oriented in the z-axis, registered, and projected to three dimensions. For cell counting, individual cells in subsequent sections were manually identified using size range and morphology criteria, then assembled as above using Neurolucida, imported to Matlab, and distances quantified automatically using custom software. For synapse counting, we first computed the fluorescence intensities profiles along a line that is nearly perpendicular to the face of the putative synapse. We counted a contact as a synapse when the overlap between pre- and postsynaptic fluorescent labels occurred at a half maximal value of less than or equal to one wavelength.

Physiology

Adult mice (eight animals older than P56) were anesthetized with ketamine/xylazine (0.13 and 0.01 mg/g body weight, respectively), with additional ketamine as needed. A cranial window was placed above cerebellum overlying trigeminal brainstem, the skin caudal to the left mystacial pad was exposed, and the buccal and marginal mandibular branches of VIIn were carefully dissected away from connective tissue, transected, and the buccal branch was

placed within a suction electrode, and isolated and stabilized with petroleum jelly. A bipolar stimulation electrode was placed across the left mystacial pad, and stimulated with a biphasic, 200 μs pulse of ~500 μA at ~1 Hz with an isolated pulse stimulator (A-M Systems Model 2100). VIIn activity was amplified at 1000× (DAM80 amplifier), digitized (ADInstruments PowerLab 8/35), and collected on a computer with associated software (LabChart 7, ADInstruments). Lesions were performed with a < 1 MΩ tungsten unipolar microelectrode (MicroProbes) with grounding electrode in nearby skin, and guided with a digital manipulator (Sutter Instruments, ROE-200 and MPC-200) according to stereotaxic coordinates (centered on −5.7 mm rostrocaudally to bregma and 1.5 mm lateral to midline).

RESULTS

Morphological evidence for a partitioning zone in spinal trigeminal complex

Olszewski (1950) proposed the gross subdivision of the trigeminal complex into four widely accepted domains. These are the rostral nucleus principalis (PrV), spinal nuclei oralis (SpVo), interpolaris (SpVi), and caudalis (SpVc) and are based on gross cytological and chemoarchitectural features (Avendano et al 2005, Kerr 1970, Ma 1991, Olszewski 1950) (Fig. 1A). The caudal boundary of SpVi abuts rostral SpVc at the beginning of the substantia gelatinosa (Fig. 1B). The boundary between SpVi and SpVc is obliquely oriented (Phelan & Falls 1989a) at or just caudal to the obex (Fukushima & Kerr 1979) (Fig. 1B,C), and was difficult to detect in the more commonly used transverse plane of section. We consider the cytoarchitecture, primary ganglionic axonal projections, and intramedullary connections of the trigeminal complex using the all three, *i.e.*, transverse, sagittal and horizontal planes of section. Given the longitudinal nature of the trigeminal complex, several of the major subdivisions are far more evident in sagittal and horizontal planes than in the more traditionally employed transverse plane.

The caudal aspect of SpVi has large neurons dorsally and medium-sized neurons ventrally and laterally, while neurons in SpVc are disposed in an approximately laminar array, relatively smaller, with dense Nissl bodies. Interestingly, neurons at the interface between SpVi and SpVc are relatively small, vertically oriented oblong cells that are comparative low in density. In transverse plane of section, neurons with these cytological features extend around the edge of the of the rostral tip of the substantia gelatinosa, medially abutting the parvocellular reticular formation (PCRt), extending laterally to the external fibers of the descending axons of the trigeminal nerve (Vn), and intermingling with the substantia gelatinosa along the lateral edge of SpVc caudally. These neurons form a narrow, ca. 70 -μm wide vertical zone in which the cells have an orientation that appears independent of those in the pars interpolaris and the pars caudalis. As the neurons appear to forming a virtual vertical "wall", and in keeping with convention, we name this anatomically distinct region *spinal trigeminal nucleus pars muralis* (SpVm).

This distinction between the pars interpolaris, muralis and caudalis were further evident in sagittal sections from transgenic mice in which inhibitory neurons expressed EGFP through different promoters. Soma were sparsely labeled in SpVm for expression driven through the vesicular Gaba transporter (VGAT; Fig. 2A), the glycine transporter (GlyT2; Fig. 2B), and glutamic acid decarboxylase (GAD67; Fig. 2C) promoters, yet strongly labeled in a mouse

line that expresses EGFP in Gaba-ergic neurons (GIN; Fig. 2D). This contrast is sharpen than and complementary to the differential cytology seen in Nissl sections (Fig. 1B). It further provides a clear means to examine the representation of SpVm in the transverse plane (Fig. 2E–L). At the most caudal position (Fig. 2E) we see neurons in *substantia gelatinosa* (SG; Fig. 2E) and the beginnings of SpVm in more rostral sections (arrows; Fig. 2F–K). We note that the identity of these cells as part of a contiguous region is difficult to discern in transverse planes, because of a dorsal-ventral and medial-lateral tilt, as opposed to sagittal (Figs. 1B and 2D) and horizontal (Fig. 1C) planes.

Cutaneous sensory afferent axons terminate at the border of SpVi and SpVc

Does trigeminal region SpVm receive input from primary afferent axons? We injected a large bolus of the anterograde tracer cholera toxin subunit B (CTb) directly into the trigeminal ganglion (10 mice) (Fig. 3A). Central afferent axons terminate robustly throughout all four major divisions of the trigeminal complex. In addition to the massive terminations within the primary trigeminal nuclei (Fig. 3B), sparse terminations were also seen in parts of the parvocellular reticular formation (Fig. 3C). However, these terminations may have been consequent to inadvertent spread of tracer into telecephalic axons independently projecting upon the reticular formation. Afferent *terminal projection fields* are especially dense in SpVi and SpVc, with distinctly different patterns of axonal terminations in these two regions. Critically, the terminal fields at the interface of SpVc and SpVi is thick and elongated dorsoventrally, suggesting that this unique cytological region receives strong input from afferent axons.

Central afferent axons of Vg project from cutaneous sensory receptors throughout the face. To dissect out the cutaneous sources of central termination zones in trigeminal brainstem, we injected CTb into parts of face innervated exclusively by the three primary branches, *i.e.*, maxillary, ophthalmic, and mandibular, of Vn (14 mice). Expectedly, central projections from each of the branches terminate in distinct and separable longitudinal bands along the dorsoventral axis throughout trigeminal brainstem, including SpVi (Fig. 3D–F). Strikingly though, the border between SpVi and SpVc is labeled exclusively by mystacial pad injection (Fig. 3D), and not by injections to supraorbital face, targeting the ophthalmic branch of Vn (Fig. 3E), or to the tongue and skin overlying the jaw, targeting the mandibular branch of Vn (Fig. 3F).

To further investigate the structure of vibrissal afferentation in the border regon between SpVi and SpVc, we labeled the cutaneous fields of afferent input of one or a few follicles by targeted injection of CTb into the mystacial pad (5 mice, same as above) (Fig. 4A). One or a few barrelettes, the cytologically distinct functional brainstem units corresponding to individual vibrissae (da Silva et al 2011, Ma 1991), were labeled as expected in SpVi and SpVc (Fig. 4B,C). Well-isolated axonal endings course in the dorsoventral axis within SpVm, filling the border between SpVi and SpVc (Fig. 4B,C). A volumetric reconstruction of the labeled terminals in the trigeminal complex shows the three-dimensional relationships of the regions labeled in the spinal trigeminal regions (Fig. 4D). Together, these results suggest that SpVm receives a set of peripheral trigeminal afferent endings originating

exclusively from the mystacial pad and this constitutes a separate region rather than a transition zone between SpVi and SpVc.

SpVm neurons project monosynaptically to lateral facial nucleus motoneurons

Motivated by the discrete termination of peripheral afferent axons in nucleus SpVm, we next asked whether neurons in this nucleus are involved in vibrissa motor output. We injected a glycoprotein-G deleted mutant rabies virus that codes GFP (GRV) into the mystacial pad of mouse line RΦGT that conditionally expresses glycoprotein-G in choline acetyltransferase (ChAT)-positive neurons at 12 days postnatal (Takatoh et al 2013) (Fig. 5A). Under this strategy, only neurons that are both retrogradely infected with G-RV and are cholinergic are competent to replicate rabies virus with the necessary glycoprotein for retrograde infection. Since VIIm is the only cholinergic brainstem nucleus that projects directly to vibrissa musculature (Takatoh et al 2013), any GFP-positive neurons outside of VIIm are necessarily monosynaptically connected to VIIm motoneurons that project to vibrissa-muscles. These motoneurons, which synapse directly onto vibrissa musculature and control vibrissae movement (Courville 1966, Klein & Rhoades 1985, Komiyama et al 1984), are positively labeled by the injection (Fig. 5B), and premotor neurons are labeled in SpVo, SpVi, and along the dorsoventral axis corresponding to SpVm (n = 4) (Fig. 5C,D). This labeling pattern dictates the candidate trigeminal regions, including SpVm, which could serve as loci for feedback from Vg to VIIm. Lastly, there was no indication of retrograde labeling of neurons within the motor trigeminus, confirming the restricted deposition of the viral tracer in the periphery to muscles innervated only by the facial motor nucleus.

Next, in order to quantify the premotor contribution of central trigeminal neurons in the adult, we injected GFP-coding pseudorabies virus (PRV), a modified transsynaptic, retrograde herpesvirus, unilaterally into the intrinsic and extrinsic musculature of the mystacial pad (32 mice) (Fig. 6A). We first characterized the infection rates of transsynaptically infected neuron populations to infer the sequential order of serial connectivity with musculature: first-order, lateral VIIm motoneurons were labeled at 48 hours (Fig. 6B) and premotor neurons innervating lateral VIIm, primarily in ipsilateral brainstem, were robustly labeled at 72 hours (Fig. 6C). The greatest density of labeled neurons throughout brainstem was within SpVm (646 of 1942 labeled neurons), while the remaining labeled neurons were primarily distributed throughout the reticular formation and along *tractus trigemini descendens* (Fig. 6C–E). Critically, SpVm contained 0.78 of the neurons in SpV (870 of 1120 neurons), while SpVc contained 0.19 (214) and SpVi contained 0.03 (36) of the neurons. The robustly labeled dendrites are morphologically similar to those seen in SpVm neurons labeled with G-RV (*cf.* Figs. 3D and 6E). Labeling was absent in SpVm on the contralateral side (Fig. 6C). A volume representation of all retrogradely labeled neurons clearly demarcates SpVm with the densest population of neurons (Fig. 6F, arrow) and labeled neuron counts indicate that the density of VIIm-projecting neurons decreases rapidly outside of this region (Fig. 6G). Taken together, these data suggest that SpVm neurons are the primary trigeminal neuronal population projecting to lateral VIIm, and that SpVm contains more VIImprojecting neurons than any other single brainstem trigeminal nucleus.

Transsynaptic and conditionally expressed viruses are powerful tools for assessing the sequential, polysynaptic connectivity of premotor neurons, yet their use is subject to systematic concerns. First, PRV is replication competent, so infection rates alone cannot precisely distinguish the number of synapses between labeled cells (Fay & Norgren 1997). Second, the tropism of both PRV and G-RV can affect the pre-motor neuron populations that are effectively labeled (Card et al 1997, Rotto-Percelay et al 1992). In particular, PRV strongly labels autonomic neurons, and likely labeled parasympathetic neurons located in the salivatory nuclei (Fig. 6B) that could receive projections from cells near SpVm (Meng & Kurose 2013). In order to verify the observed projections from SpVm to lateral VIIm, we then used a classical retrograde tracer, FluoroGold (Schmued & Fallon 1986). We microstimulated lateral VIIm to evoke exclusively vibrissal movements while ensuring the absence of non-vibrissal muscle activation, then pressure injected FluoroGold (5 mice, Fig. 6H). Lateral VIIm motoneurons were strongly labeled (Fig. 6I), and we again observed prominent retrogradely labeled neurons in SpVm (Fig. 6J). Additional labeling is seen in caudal aspects of SpVi and SpVc as well as aspects of the reticular formation (Fig. 6J), consistent with results from both PRV and G-RV injections. Taken together, these data confirm that SpVm provides the dominant premotor input to VIIm from monosynaptically innervated sensory portions of the trigeminal complex.

Vg afferent neurons monosynaptically innervate SpVm neurons that project to VIIm motoneurons

We have shown that SpVm projection neurons receive peripheral sensory afferent inputs (Fig. 2) and project to motoneurons that innervate the vibrissa musculature (Figs. 3 and 4). Yet, it remains to be shown that inputs to SpVm terminate near enough to somata or dendrites of premotor neurons to imply putative synaptic contact. To address this issue, we used a dual-label strategy in which CTb was injected into the mystacial pad and G-RV into the lateral division of ipsilateral VIIm in wild type mice after locating this region by microstimulation (3 mice, Fig. 7A,B). The retrograde virus G-RV is an ideal choice for identifying putative synaptic contacts: it exclusively traverses chemical synapses, strictly travels monosynaptically (Ugolini 2010), the coexpressed GFP allows for direct visualization of dendritic arbors (Lopez et al 2010), and low labeling density provides sufficient sparsity for counting individual synapses. The terminal field of CTb-targeted vibrissa afferent inputs was spatially coincident with G-RV infected premotor neurons in SpVm (Fig. 7C,D). Central trigeminal afferent axonal boutons, visualized with confocal microscopy, are in apposition to SpVm dendrites in individual optical sections from all three orthogonal planes (Fig. 7E,F). Linear fluorescence profiles show that synaptic elements are indeed connected at the resolution of the diffraction limit of ~ 300 nm, Fig. 7G), consistent with past analyses based on opposing elements (Corson & Erisir 2013). We counted 466 putative synapses in ~ 7.7×10^6 μm^3 of representative SpVm confocal volumes; due to sparse labeling, 1 synapse per $(25$ μm$)^3$ represents a lower bound on the density of putative synapses. Thus, primary vibrissa terminals onto SpVm projection neurons are sufficiently proximal to SpVm dendrites to suggest synaptic contact and sufficiently numerous to suggest a dominant pathway.

VIIm-projecting SpVm neurons are vGluT2+

We have shown that SpVm neurons that receive Vg sensory afferent input monosynaptically connect to VIIm motoneurons and are required for fast vibrissa reflex circuitry. Both Vg sensory afferent neurons (Lo et al 1999, Minnery & Simons 2003, Zucker & Welker 1969) and VIIm motoneurons projecting to vibrissa musculature are excitatory. While the physiological observations above suggest a net excitatory influence, what is the neurochemical signature of SpVm projection neurons projecting to VIIm motoneurons? We injected CTb into VIIm (Fig. 8A), and examined retrogradely labeled neurons in SpVm (box in Fig. 8B) using *in situ* hybridization (ISH) of excitatory and inhibitory transcripts (337 neurons in 3 mice, Fig. 8C–F, used for four different ISH markers). Neurons in SpVm labeled with CTb were primarily positive for vesicular glutamate transporter type 2 (VGluT2), a surrogate marker for the excitatory neurotransmitter glutamate (90 of 97 labeled neurons; 93% from three animals, Fig. 8F). Furthermore, CTb-labeled neurons in SpVm were entirely negative for vesicular glutamate transporter type 1 (VGluT1; 0 of 73 labeled neurons, Fig. 8E) and for inhibitory markers including vesicular inhibitory amino acid transporter (VIAAT; 0 of 79 labeled neurons, Fig. 8D) and glutamic acid decarboxylase (GAD; 0 of 88 labeled neurons, Fig. 8C). Thus, the connections from neurons in the newly identified region SpVm to the facial nucleus are exclusively excitatory.

SpVm is necessary for the vibrissa protraction reflex

The above anatomical evidence demonstrates that nucleus SpVm receives primary vibrissa input and is the predominant premotor nucleus to lateral VIIm motoneurons projecting to vibrissal musculature. Yet is this nucleus necessary for the fast circuit response seen in the vibrissa protraction reflex? To address this question, we developed a preparation to evaluate the role of SpVm in the EMG response to direct sensory stimulation of the infraorbital branch of Vn. We electrically stimulated sensory receptors of the mystacial pad in ketamine-anesthetized mice while recording with a suction electrode from transected VIIn (Fig. 9A). The VIIm response to sensory stimulus was bimodal, with peaks at 13.7 ± 1.9 ms and 37.6 ± 9.7 ms (pre-lesion) (64 trials in 3 mice, Fig. 9B); this is consistent with past work in rat, showing bimodal vibrissa muscle activation with latencies of ~ 12 ms and ~ 21 ms (Nguyen & Kleinfeld 2005). Electrolytic lesion of SpVm entirely eliminates the responses at both time points (post-lesion) (275 trials in 2 mice, Fig. 9B,C). These lesions leave trigeminal sensory input from trigeminal ganglion through nuclei principalis and spinal nuclei SpVo and SpVi intact because of the unidirectional, caudal to rostral transmission of trigeminal input. The eradication of both physiological responses suggests that SpVm is critical to both disynaptic and polysynaptic circuitry involved in fast vibrissa muscle control.

DISCUSSION

Disynaptic feedback circuitry is potentially a fundamental design principle for low-level sensory control of motor acts. Here, we have identified a novel region of the trigeminal nuclear complex that mediates disynaptic sensorimotor feedback in the vibrissa system. In particular, we have shown that projection neurons in this region, denoted SpVm, (*i*) are spatially distinct from neurons in neighboring trigeminal nuclei SpVi and SpVc (Fig. 1), (*ii*) are morphologically distinct in that they lie vertical compared to neighboring regions (Fig.

1); (*iii*) receive direct synaptic input from vertically oriented vibrissal afferent axons (Figs. 2 and 5); (*iv*) project directly to lateral VIIm motoneurons that control vibrissa musculature (Figs. 3 – 5) based on light-level albeit not electron microscopy; (*v*) are exclusively excitatory (Fig. 8); and (*vi*) are necessary for the sensory-mediated motor control of a fast vibrissa protraction reflex (Fig. 9). This brainstem circuit forms the lowest level of feedback (Fig. 10) in the hierarchy of motor control of active, vibrissa-based somatosensation (Kleinfeld et al 1999).

What is the impact of the current findings on our understanding of rodent behavior? Rodents use active sensing to explore their local environment with vibrissa movement (Brecht 2007, Kleinfeld & Deschenes 2011, Mitchinson et al 2011, Vincent 1912). Primary sensory neurons spike at up to 20 Hz as the vibrissae sweep through space in the absence of contact: a spike can genuinely or spuriously indicate contact (Leiser & Moxon 2007). This positive feedback circuit provides a means to resample a potential object, and thus to distinguish contact-generated spikes from noise in the trigeminal input. Increased EMG activity corresponds to an increase in protraction that would cause a stronger contact force in the presence of an object only. This hypothesis is supported by the observation that EMG amplitude increases during active contact, but not during free-whisking (Sachdev et al 2003). It will be interesting to identify similar modes of feedback, and the brainstem circuits that underlie them, in other systems.

Recent work on grasping motor control has revealed a disynaptic circuit in spinal cord that requires the dI3 class of interneurons for excitatory feedback (Bui et al 2013). Interestingly, this class of neurons is also vGluT2+, like SpVm neurons. In the case of the grasp reflex, gated positive feedback underlies a motor task, while in the present case feedback supports an active sensory task. While the functions differ, the similarities of this spinal circuit and the present brainstem circuit for the continuous drive provided by positive feedback suggest a general architecture.

Why should nature use disynaptic rather than monosynaptic circuits for positive feedback in vertebrates? Unchecked positive feedback can lead to runaway oscillations or exponential growth. Specialized monosynaptic circuits guard against unstable divergence by direct oppositional control: for example, the stretch reflex uses muscle spindle output to engage a reflex arc that regulates skeletal muscle length, while disynaptic inhibition through Renshaw cells provides an additional limit. In the vibrissa system, motion is limited by the mechanical constraints of vibrissa deflection, yet there is no known direct feedback from the muscles to report and control this limit to motion (Rice et al 1986). Here and in general, the interneurons in an excitatory disynaptic architecture provide a substrate for many possible mechanisms of physiological compensation for excessive positive feedback, including short-term synaptic depression and top-down inhibition. In particular, SpVm interneurons are the best known candidates for modulating sensory feedback because, first, they are not involved in feedforward sensory information processing through the lemniscal system and, second, they do not interfere with higher level motor control systems directly controlling vibrissa output through VIIm. In short, a single interneuron pool allows for circuit modulation while maintaining the shortest connection between sensory and motor systems.

Historical reevaluation of SpVm

The trigeminal ganglion innervates a broad and highly heterogeneous region of the head of vertebrates terminating in a variety of receptor organs, often specific to individual regions of the head. The domain of the head is nominally divided into three regions, the ophthalmic, maxillary and mandibular zones, also designated as V1, V2, and V3. Each region is innervated by one of the three major divisions of the trigemnal nerve and ganglion. The trigeminal ganglion contains a heterogeneous collection of sensory neurons of varying sizes and molecular profiles (Lazarov 2002), innervating a diverse range of peripheral sensory organs. The trigeminal ganglion projects upon a complex group of subnuclei that extends the length of the pons and medullary region. The individual divisions of the trigeminal ganglion terminate in varying density and manner along the length of the trigeminal complex. Each branch of the trigeminal nerves maintain a relatively distinct and separate zone of termination along their dorsoventral and mediolateral axes, as they distribute along the rostrocaudal length of the various divisions of the trigeminal complex. In general, however, in rodents the mandibular division, V3, lies most dorsally and medially; the maxillary division, V2, lies somewhat more ventrally and laterally; the ophthalmic division, V1, lies most ventrolaterally. However, even within the domain of each field of distribution, the target zone of termination is highly heterogeneous, consisting of multiple small subnuclei of differing cytoarchitecture and patterns of termination of the primary sensory inputs. Cajal (Cajal 1909) proposed subdividing the trigeminal complex into an ascending branch and a descending one. In recognition of the complexity of these multiple subdivisions, Olszewski (Olszewski 1950) proposed the gross subdivision into four domains: the rostral nucleus principalis (PrV) and spinal nuclei oralis (SpVo), interpolaris (SpVi), and caudalis (SpVc) (Fig. 1A).

Has SpVm been overlooked previously? Olszewski's (Olszewski 1950) predecessors and contemporaries, as well as more recent anatomists, have delineated many different variations of spinal nuclear organization on the basis of cytoarchitecture (Astrom 1953, Krieg 1950, Phelan & Falls 1989a, Phelan & Falls 1989b, Torvik 1956). Interestingly, a reevaluation of single axon reconstructions of peripheral afferent axonal terminations in trigeminal brainstem reveal a distinct terminal morphology in nucleus SpVm, at the obex (Hayashi 1980) (his figure 1A) and a prominent change in collateral distribution at this location (Hayashi 1980) (his figure 2). This has been summarized in past work (Hayashi 1985) (his figure 10) though the extent of these differences in termination is disputed (Shortland et al 1995). Thus, consistent though unrecognized evidence for a discrete zone between SpVi and SpVc exists in the literature.

Neurons located near the transition region between SpVi and SpVc have been implicated in other orofacial reflexes, including tear production and eyeblink (Kurose & Meng 2013, Meng & Kurose 2013). Neurons at the ventral aspect of this region are necessary for tear production and respond to drying or wetting of the corneal surface and to mechanical stimulation of the face (Hirata et al 2004). Further, some of these cells project to the superior salivatory nucleus, a region immediately rostral to the facial nucleus that contains preganglionic efferents for autonomic functions. There is further evidence that neurons near the transition region between SpVi and SpVc project to eyelid motoneurons in the dorsal

facial nucleus (Morcuende et al 2002, Zerari-Mailly et al 2003) and control eyeblink (Henriquez & Evinger 2007). Together with the present results, *pars muralis* emerges as a trigeminal nucleus that may be specialized for mediating oligosynaptic reflex arcs that are localized to the brainstem.

Anatomical similarities between SpVc and spinal cord have been described (Gobel et al 1981, Jacquin et al 1986), prompting some to adopt the term medullary dorsal horn in place of SpVc. In this scheme, the analog of substantia gelatinosa, or Rexed lamina II, sits on the lateral edge of SpVc, and wraps medially toward PCRt as SpVc abuts SpVi. In our nomenclature, nucleus SpVm might be analogous to substantia gelatinosa, Rexed lamina II, as it sits on the posterior edge of spinal cord. However, four lines of evidence suggest that SpVm is distinct from a putative substantia gelatinosa analog. First, the cytoarchitecture of SpVm does not show a gelatinous texture, as a consequence of the large number of myelinated fibers in this region (see tissue refractility in Fig. 1). Second, the vast majority of Vg afferent endings and VIIm-projecting neurons lie only in the most rostral portion of what was previously called rostral SpVc (Figs. 2F,G, 3C, and 4C–F). Third, substantia gelatinosa is not labeled by FluoroGold injected in VIIm or by transsynaptic retrograde viruses in the face (Figs. 3 and 4). Finally, analogous dI3 interneurons sit primarily in Rexed laminae IV, V, and VI (Bui et al 2013). Taken together, while SpVm does not explicitly fit the laminar structure of the proposed medullary dorsal horn schema, this general circuit architecture is strikingly similar between brainstem and cord.

ACKNOWLEDGMENTS

ROLE OF AUTHORS

All authors had full access to all of the data in this study and take responsibility for the integrity of the data and the accuracy of the data analysis. M.D., H.J.K., D.K. and D.W.M. designed the study, M.D., T.H., D.W.M., J.D.M. and F.W. carried out the experiments, D.W.M. analyzed and summarized the data with input from H.J.K. and D.K., D.K. and D.W.M. wrote the manuscript, and D.K. dealt with the myriad of university organizations that govern animal health and welfare, surgical procedures, and laboratory health and safety issues that include specific oversight of chemicals, controlled substances, human cell lines, lasers, and viruses.

Abbreviations

CTb	Cholera toxin, subunit B
DAB	Diaminobenzidne
G-RV	Glycoprotein-deleted rabies virus
GAD67	glutamic acid decarboxylase

GFP	Green fluorescent protein
GlyT2	glycine transporter
IoN	Infraorbital branch of the trigeminal nerve
IRT	Intermediate reticular nucleus
ISH	*In situ* hybridization
PrV	Principal nucleus of the trigeminal nerve
PRV	Pseudorabies virus
RΦGT	Floxed-stop glycoprotein × Chat-Cre crossed transgenic mouse
SpV	Spinal nucleus of the trigeminal brainstem
SpVc	Spinal nucleus caudalis
SpVi	Spinal nucleus interpolaris
SpVm	Spinal nucleus muralis (new)
SpVo	Spinal nucleus oralis
Vg	Trigeminal ganglion
VGAT	Vesicular Gaba transporter
VGluT1/2	Vesicular glutamate transporter 1/2
VIAAT	Vesicular inhibitory amino acid transporter
VIIm	Facial motor nucleus
VIIn	Facial nerve
Vm	Motor division of trigeminal nerve
Vn	Trigeminal nerve

REFERENCES

Angel MJ, Jankowska E, McCrea DA. Candidate interneurones mediating group I disynaptic EPSPs in extensor motoneurones during fictive locomotion in the cat. Journal of Physiology. 2005; 563(2): 597–610. [PubMed: 15618278]

Angelucci A, Clasca F, Sur M. Anterograde axonal tracing with the subunit B of cholera toxin: A highly sensitive immunohistochemical protocol for revealing fine axonal morphology in adult and neonatal brains. Journal of Neuroscience Methods. 1996; 65:101–112. [PubMed: 8815303]

Arvidsson J. Somatotopic organization of vibrissae afferents in the trigeminal sensory nuclei of the rat studied by transganglionic transport of HRP. Journal of Comparative Neurology. 1982; 211:84–92. [PubMed: 6983532]

Astrom KE. On the central course of afferent fibres in the trigeminal, facial, glossophryngeal, and vagal nerves and their nuclei in the mouse. Acta Physiologica Scandinavica. 1953; 29:209–320.

Avendano C, Machin R, Bermejo PE, Lagares A. Neuron numbers in the sensory trigeminal nuclei of the rat: A GABA- and glycine-immunocytochemical and stereological analysis. Journal of Comparative Neurology. 2005; 493:538–553. [PubMed: 16304625]

Bellavance MA, Demers M, Deschenes M. Feedforward inhibition determines the angular tuning of vibrissal responses in the principal trigeminal nucleus. Journal of Neuroscience. 2010; 30:1057–1063. [PubMed: 20089914]

Brecht M. Barrel cortex and whisker-mediated behaviors. Current Opinion in Neurobiology. 2007; 17:408–416. [PubMed: 17702566]

Bui TV, Akay T, Loubani O, Hnasko TS, Jessell TM, Brownstone RM. Circuits for grasping: Spinal dI3 interneurons mediate cutaneous control of motor behavior. Neuron. 2013; 78:191–204. [PubMed: 23583114]

Burke, RE. Spinal cord: Ventral horn. In: Shepherd, GM., editor. The Synaptic Organization of the Brain. 5 th edition. Oxford: Oxford University Press; 2004. p. 79-123.

Cajal, SRy. Chapter XXXI: The trigeminal or Vth cranial nerve. New York: Oxford University Press; 1905. p. 704-729.

Cajal, SRY. Histologie du Système Nerveux de l'Homme et des Vertébrés. Paris: Maloine; 1909.

Card JP, Enquist LW, Miller AD, Yates BJ. Differential tropism of pseudorabies virus for sensory neurons in the cat. Journal of Neurovirology. 1997; 3:49–61. [PubMed: 9147821]

Corson JA, Erisir A. Monosynaptic convergence of chorda tympani and glossopharyngeal afferents onto ascending relay neurons in the nucleus of the solitary tract: A high-resolution confocal and correlative electron microscopy approach. Journal of Comparative Neurology. 2013; 521:2907–2926. [PubMed: 23640852]

Courville J. The nucleus of the facial nerve: The relation between cellular groups and peripheral branches of the nerve. Brain Research. 1966; 1:338–354. [PubMed: 5961910]

da Silva S, Hasegawa H, Scott A, Zhou X, Wagner AK, et al. Proper formation of whisker barrelettes requires periphery-derived Smad4-dependent TGF-beta signaling. Proceedings of the National Academy of Sciences USA. 2011; 22:3395–3400.

Erzurumlu RS, Killackey HP. Efferent connections of the brainstem trigeminal complex with the facial nucleus of the rat. Journal of Comparative Neurology. 1979; 188:75–86. [PubMed: 500855]

Fay RA, Norgren R. Identification of rat brainstem multisynaptic connections to the oral motor nuclei in the rat using pseudorabies virus. II. Facial muscle motor systems. Brain Research Reviews. 1997; 25:276–290. [PubMed: 9495559]

Fukushima T, Kerr FW. Organization of trigeminothalamic tracts and other thalamic afferent systems of the brainstem in the rat: Presence of gelatinosa neurons with thalamic connections. Journal of Comparative Neurology. 1979; 183:169–184. [PubMed: 758332]

Furuta T, Nakamura K, Deschenes M. Angular tuning bias of vibrissa-responsive cells in the paralemniscal pathway. Journal of Neuroscience. 2006; 26:10548–10557. [PubMed: 17035540]

Furuta T, Timofeeva E, Nakamura K, Okamoto-Furuta K, Togo M, et al. Inhibitory gating of vibrissal inputs in the brainstem. Journal of Neuroscience. 2008; 28:1789–1797. [PubMed: 18287495]

Gibson JJ. Observations on active touch. Psychological Review. 1962; 69:477–491. [PubMed: 13947730]

Gobel, S.; Hockfield, S.; Ruda, MA. Anatomical similarities between medullary and spinal dorsal horns. In: Kawamura, Y.; Dubner, R., editors. Oral-facial sensory and motor functions. Quintessence; 1981.

Graf W, Gerrits N, Yatim-Dhiba N, Ugolini G. Mapping the oculomotor system: the power of transneuronal labelling with rabies virus. European Journal of Neuroscience. 2002; 15:1557–1562. [PubMed: 12028367]

Hattox AM, Priest CA, Keller A. Functional circuitry involved in the regulation of whisker movements. Journal of Comparative Neurology. 2002; 442:266–276. [PubMed: 11774341]

Hayashi H. Distributions of vibrissae afferent fiber collaterals in the trigeminal nuclei as revealed by intra-axonal injection of horseradish peroxidase. Brain Research. 1980; 183:442–446. [PubMed: 7353148]

Hayashi H. Morphology of central terminations of intra-axonally stained, large, myelinated primary afferent fibers from facial skin in the rat. Journal of Comparative Neurology. 1985; 237:195–215. [PubMed: 2993374]

Henriquez VM, Evinger C. The three-neuron corneal reflex circuit and modulation of second-order corneal responsive neurons. Experimental Brain Research. 2007; 179:691–702. [PubMed: 17216149]

Hirata H, Okamoto K, Tashiro A, Bereiter DA. A novel class of neurons at the trigeminal subnucleus interpolaris/caudalis transition region monitors ocular surface fluid status and modulates tear production. Journal of Neuroscience. 2004; 24:4224–4232. [PubMed: 15115818]

Holstege G, van Ham JJ, Tan J. Afferent projections to the orbicularis oculi motoneuronal cell group: An autoradiographical tracing study in the cat. Brain Research. 1986; 374:306–320. [PubMed: 3719340]

Isokawa-Akesson M, Komisaruk BR. Difference in projections to the lateral and medial facial nucleus: Anatomically separate pathways for rhythmical vibrissa movement in rats. Experimental Brain Research. 1987; 65:385–398. [PubMed: 3556466]

Jacquin M, Barcia M, Rhoades RW. Structure-function relationships in rat brainstem subnucleus interpolaris: IV. Projection neurons. Journal of Comparative Neurology. 1989a; 282:45–62. [PubMed: 2708593]

Jacquin MF, Golden J, Rhoades RW. Structure-function relationships in rat brainstem subnucleus interpolaris: III. Local circuit neurons. Journal of Comparative Neurology. 1989b; 282:24–44. [PubMed: 2708592]

Jacquin MF, Woerner D, Szczepanik AM, Riecker V, Mooney RD, Rhoades RW. Structure-function relationships in rat brainstem subnucleus interpolaris. I. Vibrissa primary afferents. Journal of Comparative Neurology. 1986; 243:266–279. [PubMed: 3944280]

Jankowska E. Interneuronal relays in spinal pathways from proprioceptors. Progress in Neurobiology. 1992; 38:335–378. [PubMed: 1315446]

Kerr FWL. The divisional organization of afferent fibres of the trigeminal nerve. Brain. 1963; 86:721. [PubMed: 14090525]

Kerr FWL. The fine structure of the subnucleus caudalis of the trigeminal nerve. Brain Research. 1970; 23:129–145. [PubMed: 5476762]

Kiehn O. Locomotor circuis in the mammalian cord. Annual Review of Neuroscience. 2006; 29:279–306.

Kirkwood BYPA, Sears TA. Excitatory post-synaptic potentials from single muscle spindle afferents in external intercostal motoneurones of the cat. Journal of Physiology. 1982; 322:287–314. [PubMed: 6461757]

Klein B, Rhoades R. The representation of whisker follicle intrinsic musculature in the facial motor nucleus of the rat. Journal of Comparative Neurology. 1985; 232:55–69. [PubMed: 3973083]

Kleinfeld D, Ahissar E, Diamond ME. Active sensation: Insights from the rodent vibrissa sensorimotor system. Current Opinion in Neurobiology. 2006; 16:435–444. [PubMed: 16837190]

Kleinfeld D, Berg RW, O'Connor SM. Anatomical loops and their electrical dynamics in relation to whisking by rat. Somatosensory and Motor Research. 1999; 16:69–88. [PubMed: 10449057]

Kleinfeld D, Deschênes M. Neuronal basis for object location in the vibrissa scanning sensorimotor system. Neuron. 2011; 72:455–468. [PubMed: 22078505]

Komiyama M, Shibata H, Suzuki T. Somatotopic representation of facial muscles within the facial nucleus of the mouse. Brain Behavior Evolution. 1984; 24:144–151.

Krieg WJS. Subdivisions of the nuclei of the spinal trigeminal tract in the rat. Journal of Comparative Neurology. 1950; 92:401–413. [PubMed: 15422069]

Kurose M, Meng ID. Corneal dry-responsive neurons in the spinal trigeminal nucleus respond to innocuous cooling in the rat. Journal of Neurophysiology. 2013; 109:2517–1522. [PubMed: 23446686]

Lazarov NE. Comparative analysis of the chemical neuroanatomy of the mammalian trigeminal ganglion and mesencephalic trigeminal nucleus. Progress in Neurobiology. 2002; 66:19–59. [PubMed: 11897404]

Leiser SC, Moxon KA. Responses of trigeminal ganglion neurons during natural whisking behaviors in the awake rat. Neuron. 2007; 53:117–133. [PubMed: 17196535]

Li YG, Takada M, Keneko T, Mizuno N. Distribution of GABAergic and glycinergic premotor neurons projecting to the facial and hypoglossal nuclei in the rat. Journal of Comparative Neurology. 1997; 378:283–294. [PubMed: 9120066]

Lo FS, Guido W, Erzurumlu RS. Electrophysiological properties and synaptic responses of cells in the trigeminal principal sensory nucleus of postnatal rats. Journal of Neurophysiology. 1999; 82:2765–2775. [PubMed: 10561443]

Lopez IP, Salin P, Kachidian P, Barroso-Chinea P, Rico AJ, et al. The added value of rabies virus as a retrograde tracer when combined with dual anterograde tract-tracing. Journal of Neuroscience Methods. 2010; 194:21–27. [PubMed: 20096304]

Ma PM. The barrelettes-architectonic vibrissal representations in the brainstem trigeminal complex of the mouse: Normal structural organization. Journal of Comparative Neurology. 1991; 309:161–199. [PubMed: 1715890]

Marfurt CF. The central projections of trigeminal primary afferent neurons in the cat as determined by the tranganglionic transport of horseradish peroxidase. Journal of Comparative Neurology. 1981; 203:785–798. [PubMed: 6173403]

Meng ID, Kurose M. The role of corneal afferent neurons in regulating tears under normal and dry eye conditions. Experimental Eye Research. 2013; 117:79–87. [PubMed: 23994439]

Minnery BS, Simons DJ. Response properties of whisker-associated trigeminothalamic neurons in rat nucleus principalis. Journal of Neurophysiology. 2003; 89:40–56. [PubMed: 12522158]

Mitchinson B, Grant RA, Arkley K, Rankov V, Perkn I, Prescott TJ. Active vibrissal sensing in rodents and marsupials. Philosophical Transaction of the Royal Society of London B - Biological Science. 2011; 366:3037–3048.

Morcuende S, Delgado-Garcia JM, Ugolini G. Neuronal premotor networks involved in eyelid responses: retrograde transneuronal tracing with rabies virus from the orbicularis oculi muscle in the rat. Journal of Neuroscience. 2002; 22:8808–8818. [PubMed: 12388587]

Nelson ME, MacIver MA. Sensory acquisition in active sensing systems. Comparative of Physiology A. Sensory, Neural and Behavioral Physiology. 2006; 192:573–586.

Nguyen Q-T, Kleinfeld D. Positive feedback in a brainstem tactile sensorimotor loop. Neuron. 2005; 45:447–457. [PubMed: 15694330]

Oliva AA Jr, Jiang M, Lam T, Smith TL, Swann JW. Novel hippocampal interneuronal subtypes identified using transgenic mice that express green fluorescent protein in GABAergic interneurons. Journal of Neuroscience. 2000; 20:3354–3368. [PubMed: 10777798]

Olszewski J. On the anatomical and functional organization of the spinal trigeminal nucleus. Journal of Comparative Neurology. 1950; 92:401–413. [PubMed: 15422069]

Panneton WM, Martin GF. Brainstem projections to the facial nucleus of the opossum. A study using axonal transport techniques. Brain Research. 1983; 267:19–33. [PubMed: 6190536]

Pellegrini JJ, Horn AKE, Evinger C. The trigeminally evoked blink reflex: I. Neuronal circuits. Experimental Brain Research. 1995; 107:166–180. [PubMed: 8773237]

Phelan KD, Falls WM. An analysis of the cyto-and myeloarchitectonic organization of trigeminal nucleus interpolaris in the rat. Somatosensory & Motor Research. 1989a; 6:333–366. [PubMed: 2756802]

Phelan KD, Falls WM. The interstitial system of the spinal trigeminal tract in the rat: Anatomical evidence for morphological and functional heterogeneity. Somatosensory & Motor Research. 1989b; 6:367–399. [PubMed: 2547273]

Pinganaud G, Bernat I, Buisseret P, Buisseret-Delmas C. Trigeminal projections to hypoglossal and facial motor nuclei in the rat. Journal of Comparative Neurology. 1999; 415:91–104. [PubMed: 10540360]

Powers WT. Feedback: Beyond behaviorism. Science. 1973; 179:351–356. [PubMed: 4682961]

Rice FL. Structure, vascularization, and innervation of the mystacial pad of the rat as revealed by the lectin Griffonia simplicifolia. Journal of Comparative Neurology. 1993; 337:386–399. [PubMed: 8282849]

Rice FLA, Mance A, Munger BL. A comparative light microscopic analysis of the sensory innervation of the mystacial pad. I. Innervation of vibrissal follicle-sinus complexes. Journal of Comparative Neurology. 1986; 252:154–174. [PubMed: 3782505]

Rice FL, Fundin BT, Arvidsson J, Aldskogius H, Johansson O. Comprehensive immunofluoresce and lectin binding study of the innervation of vibrissae follicle sinus complexes on the mystacial pad of the rat. Journal of Comparative Neurology. 1997; 385:149–184. [PubMed: 9268122]

Rotto-Percelay DM, Wheeler JG, Osorio FA, Platt KB, Loewy AD. Transneuronal labeling of spinal interneurons and sympathetic preganglionic neurons after pseudorabies virus injections in the rat medial gastrocnemius muscle. Brain Research. 1992; 574:291–306. [PubMed: 1322222]

Sachdev RNS, Berg RW, Champney G, Kleinfeld D, Ebner FF. Unilateral vibrissa contact: Changes in amplitude but not timing of rhythmic whisking. Somatosensory & Motor Research. 2003; 20:162–169.

Schmued LC, Fallon JH. Fluoro-Gold: A new fluorescent retrograde axonal tracer with numerous unique properties. Brain Research. 1986; 377:147–154. [PubMed: 2425899]

Schroeder CE, Wilson DA, Radman T, Scharfman H, Lakatos P. Dynamics of active sensing and perceptual selection. Current Opinion in Neurobiology. 2010; 20:172–176. [PubMed: 20307966]

Shortland PJ, DeMaro JA, Jacquin MF. Trigeminal structure-function relationships: A reevaluation based on long-range staining of a large sample of brainstem a beta fibers. Somatosensory & Motor Research. 1995; 12:249–275. [PubMed: 8834301]

Skinner, BF. The behavior of organisms. New York: 1938.

Takatoh J, Nelson A, Zhou X, Bolton MM, Ehlers MD, et al. New modules are added to vibrissal premotor circuitry with the emergence of exploratory whisking. Neuron. 2013; 77:346–360. [PubMed: 23352170]

Takeuchi Y, Nakano K, Uemura M, Matsuda K, Matsushima R, Mizuno N. Mesencephalic and pontine afferent fiber system to the facial nucleus in the cat: A study using the horseradish and silver impregnation techniques. Experimental Neurology. 1979; 342:330–342. [PubMed: 488225]

Tamamaki N, Yanagawa T, Tomioka R, Miyazaki J, Obata K, Kaneko T. Green fluorescence protein expression and colocalization with calretinin, parvalbumin, and somatostatin in the GAD67-GFP knock-in mouse. Journal of Comparative Neurology. 2003; 40:60–79. [PubMed: 14574680]

Torvik A. Afferent connections to the sensory trigeminal nuclei, the nucleus of the solitary tract and adjacent structures. An experimental study in the rat. Journal of Comparative Neurology. 1956; 106:51–132. [PubMed: 13398491]

Travers JB, Norgen R. Afferent projections to the oral motor nuclei in the rat. Journal of Comparative Neurology. 1983; 220:280–298. [PubMed: 6315785]

Ugolini G. Advances in viral transneuronal tracing. Journal of Neuroscience Methods. 2010; 194:2–20. [PubMed: 20004688]

van Ham JJ, Yeo CH. Trigeminal inputs to eyeblink motoneurons in the rabbit. Experimental Neurology. 1996; 142:244–257. [PubMed: 8934557]

Vincent SB. The function of the vibrissae in the behavior of the white rat. Behavior Monographs. 1912; 1:7–81.

Zeilhofer HU, Studler B, Arabadzisz D, Schweizer C, Ahmadi S, et al. Glycinergic neurons expressing enhanced green fluorescent protein in bacterial artificial chromosome transgenic mice. Journal of Comparative Neurology. 2005; 482:123–141. [PubMed: 15611994]

Zerari-Mailly F, Dauvergne C, Buisseret P, Buisseret-Delmas C. Localization of trigeminal, spinal, and reticular neurons involved in the rat blink reflex. Journal of Comparative Neurology. 2003; 467:173–184. [PubMed: 14595767]

Zhao S, Ting JT, Attalah HE, Qiu L, Tan J, et al. Cell-type specific optogenetic mice for dissecting neural circuitry function. Nature Methods. 2011; 8:745–752. [PubMed: 21985008]

Zucker E, Welker WI. Coding of somatic sensory input by vibrissae neurons in the rat's trigeminal ganglion. Brain Research. 1969; 12:134–156.
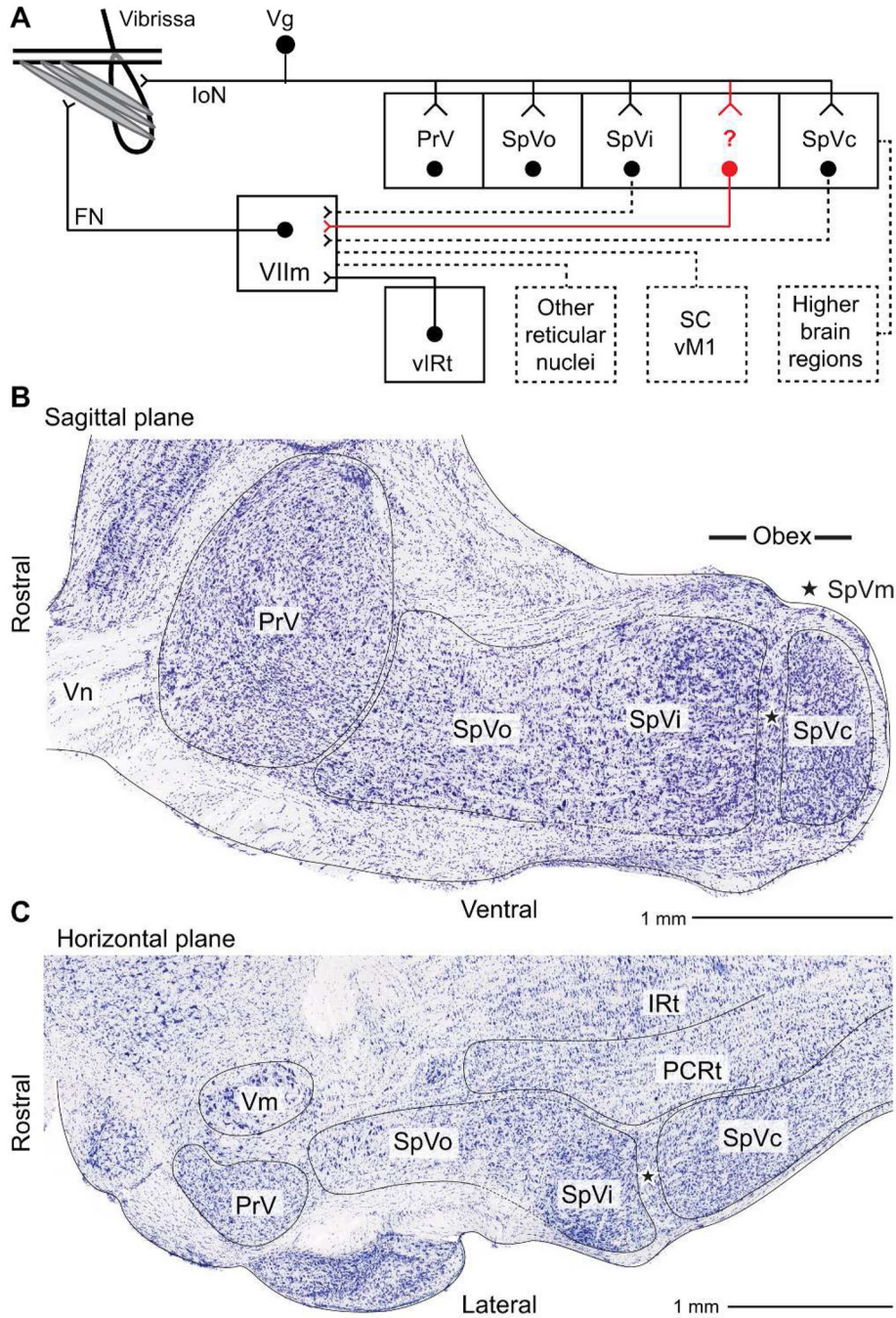
Figure 1. Organization of the trigeminal nuclei
A: Schematic of trigeminal brainstem nuclei. Sensory afferent neurons transmit signals from the mystacial pad via the infraorbital nerve (IoN) of the maxillary branch of the trigeminal nerve (Vn), through the trigeminal ganglion (Vg), and terminate throughout the trigeminal nuclear complex, which includes the principal trigeminal nucleus (PrV), and the spinal trigeminal nuclei oralis (SpVo), interpolaris (SpVi), and caudalis (SpVc). A fifth nucleus, spinal trigeminal nuclei muralis (SpVm) and its connections are the subject of this report (red-colored). Neurons in the trigeminal nuclear complex project within trigeminal

brainstem, to facial motor nucleus (VIIm), and to higher brain areas in thalamus, cerebellum, and superior colliculus. VIIm motoneurons also receive input from a vibrissa pattern generator in the vibrissa zone of the intermediate reticular formation (vIRt) and from disparate cortical and subcortical nuclei. VIIm motoneurons project to extrinsic and intrinsic musculature of the face for vibrissa motor control. **B:** Nuclear outlines, based on classical cytological differences, overlaying Nissl-stained sections in the sagittal and horizontal planes. The distinct gross morphology of each of the trigeminal nuclei and several neighboring nuclei are outlined. PCRt refers to the parvocellular region of the reticular formation, IRt to the intermediate region of the reticular formation, and Vm to the trigeminal motor nucleus. The star (★) highlights the region that contains SpVm.
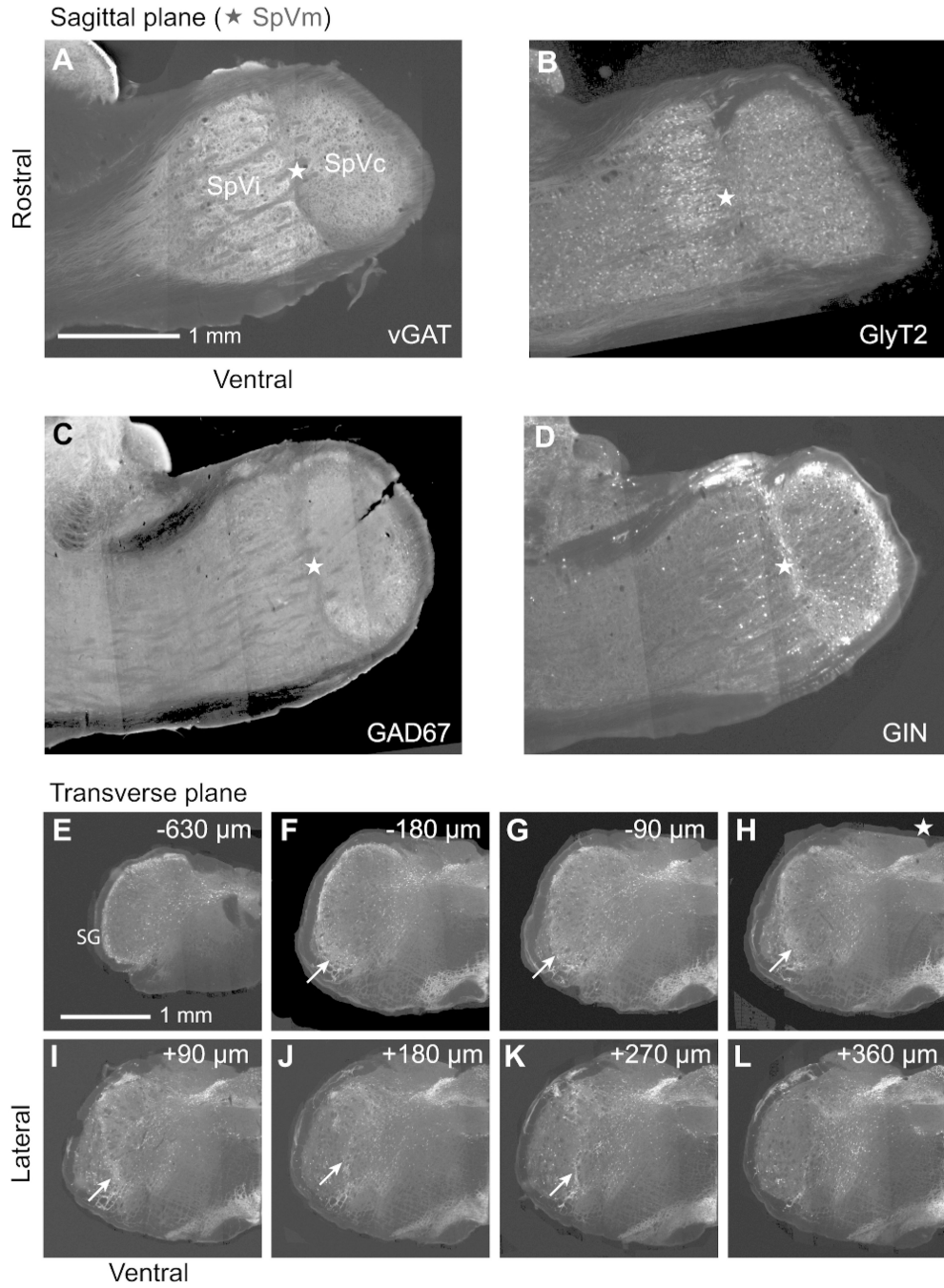
Figure 2. Sagittal and transverse views of inhibitory neurons within and near SpVm
A–D: Sagittal sections from transgenic animals that express EGFP driven by particualr promoters: VGAT is the vesicular Gaba transporter, GlyT2 is the glycine transporter, GAD67 is the glutamic acid decarboxylase, and GIN is a line with eGFP-expressing inhibitory neurons. The star (★) highlights the region that contains SpVm. **E**: Transverse sections from GIN animals; SG is *substantia gelatinosa* and the arrows point to SpVm. Distances are from the location of SpVm in panel F with positive numbers in the rostral direction.
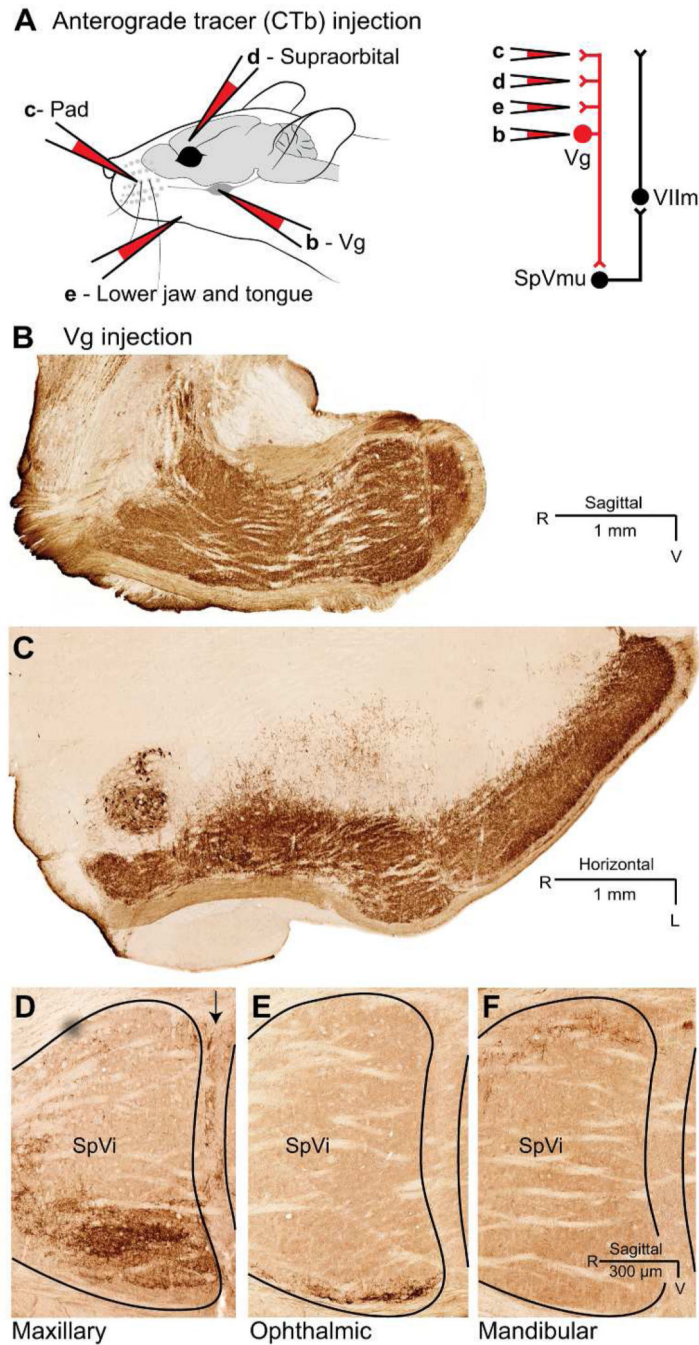
Figure 3. Sensory afferent axons terminate in the spinal trigeminal nuclei
A: Schematic of the location of cholera toxin B (CTb) injections. The letter above each injection pipette indicates the panel it represents. Red-colored connections in the circuit diagram indicate the projections under examination. Injections were performed in independent animals. **B–C:** Representative sagittal (panel B) and horizontal (panel C) sections of trigeminal brainstem after bolus injections of CTb into Vg. Diaminobenzidine reaction product (dark brown) indicates axons and terminals, which occur throughout the trigeminal nuclear complex, Vm, and PCRt. **D–E:** Central afferent axonal terminations

following focal injections of CTb in the regions of face innervated by the three trigeminal nerve branches: maxillary (panel D), ophthalmic (panel E), and mandibular (panel F), The border between nuclei SpVi and SpVc shows arborization after mystacial pad injection only, which labels the maxillary branch exclusively. Outlines show SpVi and the rostral edge of SpVc.
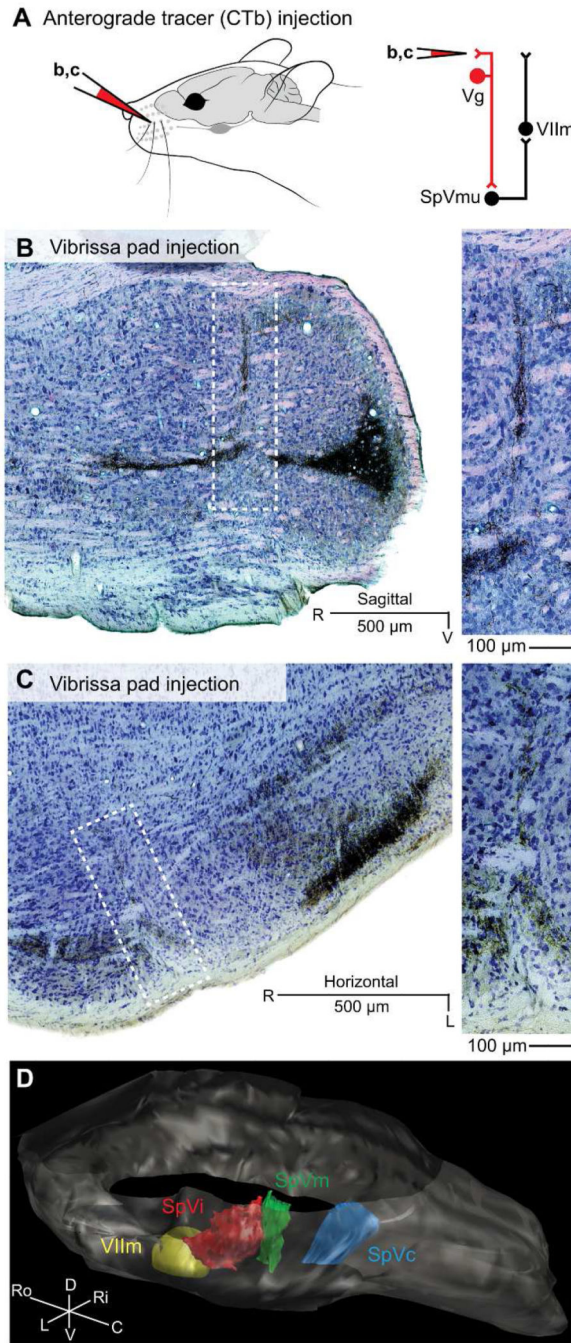
Figure 4. Trigeminal brainstem following focal injection of CTb into one or a few follicles of the mystacial pad

A: Schematic of the location of cholera toxin B (CTb) injections. Red-colored connections in the circuit diagram indicate the projections under examination. Injections were performed in independent animals. **B:** Representative sagittal section. Dark product reaction against CTb reveals fine terminal structure of primary somatosensory inputs in trigeminal brainstem; Giemsa is used as a counterstain to cell bodies. Inset: Magnified portion of the border between SpVi and SpVc reveals a spatially localized peripheral termination zone of

sensory inputs. **C:** Horizontal section, as in panel B. Spatially localized somatosensory inputs arborize on the border between nuclei SpVi and SpVc, in several laminar divisions of nucleus SpVc, and in part of the barrelette field of nucleus SpVi. **D:** Representative volumetric reconstruction of brainstem from the same data set shown in panel C, showing axonal innervation in trigeminal brainstem after focal CTb injection into mystacial pad. The view is from the left, caudal to and above bregma. For clarity, terminations rostral to SpVi are not shown.
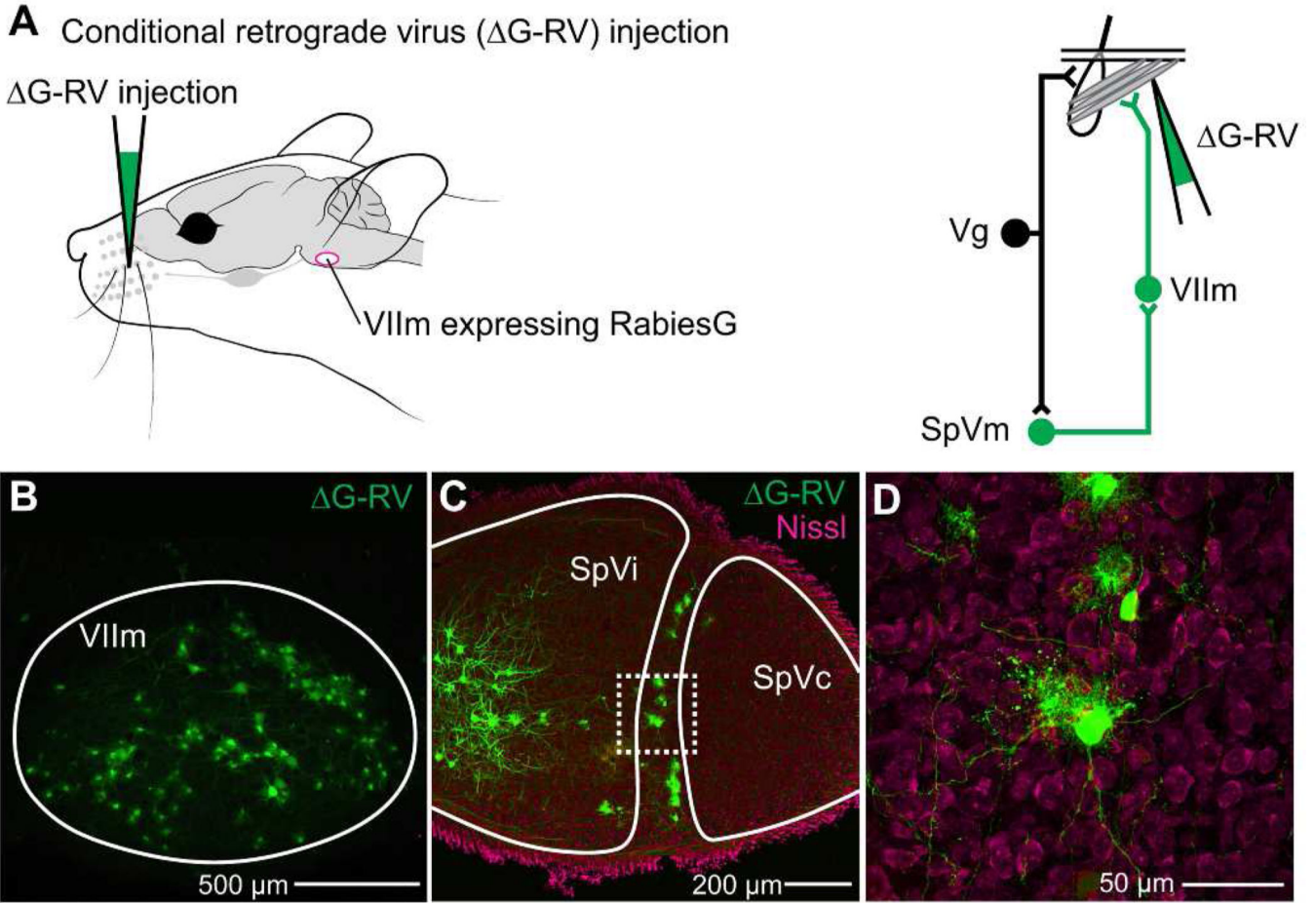
Figure 5. Retrograde labeling of SpVm by modified Rabies virus
A: Injection strategy for premotor neuron labeling. G-RV was pressure injected into the facial musculature of juvenile RΦGT mice and is transported transynaptically to facial motoneurons. Rabies glycoprotein is only expressed in the presence of cholineacetyltransferase, which is present in VIIm motoneurons using the Cre-Lox system. This permits active rabies to be recapituated in labeled facial motoneurons for subsequent labeling of premotoneurons. Schematic of vibrissa and the circuit under investigation are used throughout. **B:** Rabies-labeled (green) motoneurons are robustly labeled in lateral VIIm (sagittal section). **C:** Monosynaptically-connected premotor neurons in nuclei SpVo, SpVi, and SpVm, labeled by G-RV (green) and counterstained with a fluorescent Nissl (Neurotrace red). **D:** Magnified images of a set of SpVm neurons (box in panel C), showing dendritic arborization and strict alignment along the border of SpVi and SpVc.
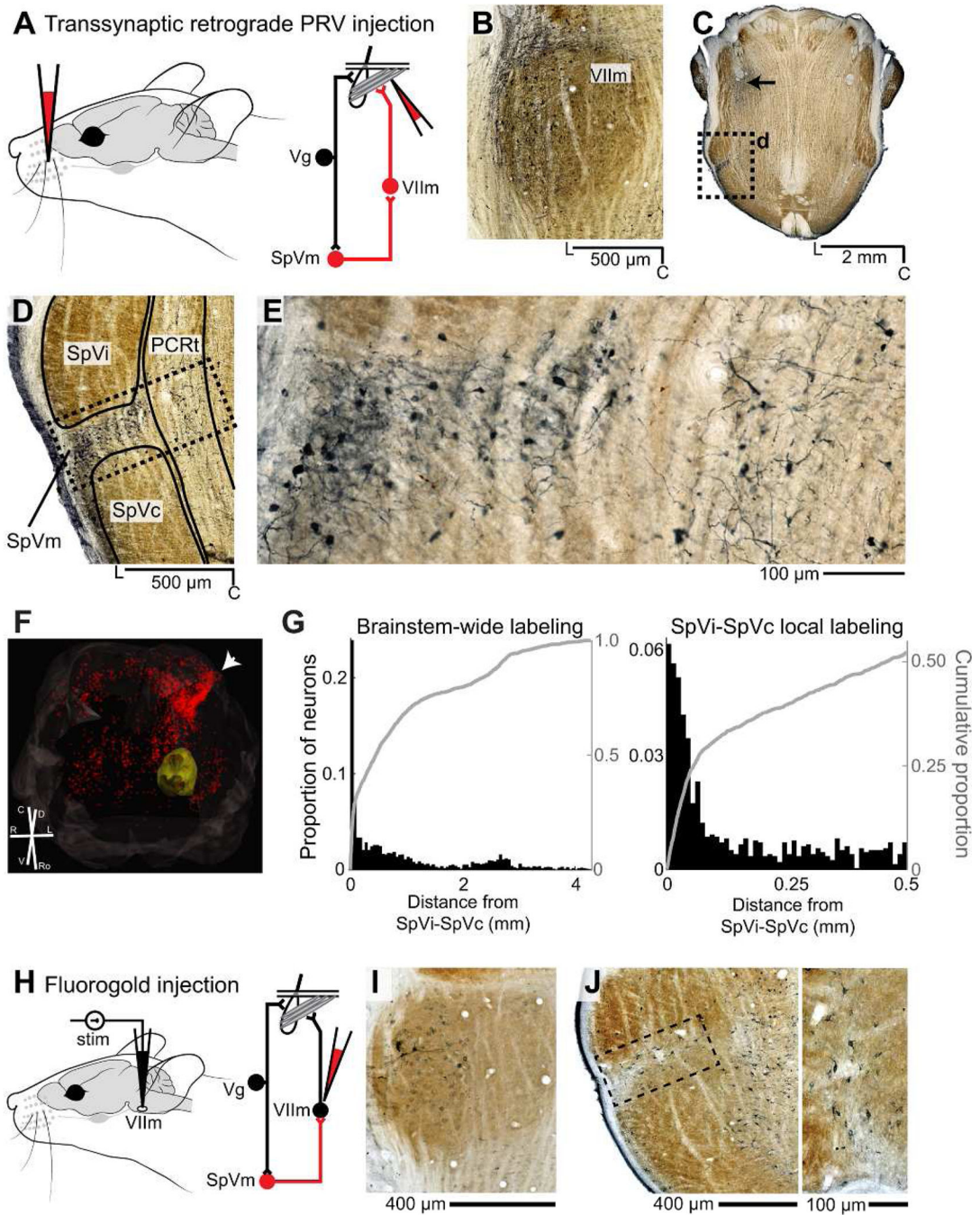
Figure 6. Retrograde labeling of SpVm by pseudorabies virus and FluoroGold
A: Injection strategy. Pseudorabies virus (PRV) was injected into the intrinsic and extrinsic musculature of the left mystacial pad. **B:** Positive labeling in lateral VIIm ipsilateral to injection after 48 hours, horizontal slice. Large motoneurons are robustly labeled, as are parts of superior salivatory nucleus, rostral to VIIm. Medial divisions of VIIm are unlabeled. **C:** Representative brainstem slice showing PRV-positive neuron labeling. The most robust and densest labeling is in ipsilateral SpVm (box). PRV labeling is also visible in the *genu* of VII at this level, dorsal to VIIm (arrow). **D:** Magnification of box in **c**. Ipsilateral nuclei

SpVm and PCRt are robustly labeled. **E:** Magnification of box in Panel D. VIIm-projecting SpVm neurons (left) are smaller and have more confined dendrites than the Golgi-like labeled neurons in PCRt (right). **F:** Volumetric reconstruction of brainstem from aligned, serial sections (see methods). Red dots indicate locations of 2251 PRV-positive, non-VIIm neurons, of which 29% (646 of 2251) are in ipsilateral SpVm (white arrowhead). VIIm (outlined in yellow) contains primary labeled motoneurons whose individual cell bodies are not shown for clarity; brainstem is outlined in gray. **G:** Distribution of PRV-positive neurons relative to the centerline between SpVi and SpVc (arrow in panel F). The top distribution has a bin size of 50 μm while the bottom has a bin size of 10 μm. **H:** FluoroGold injection strategy. After targeting lateral VIIm by eliciting vibrissa movement in response to microstimulation, tracer was iontophoresed. **I:** FluoroGold labeling in VIIm motoneurons. Lateral VIIm is strongly labeled, while medial VIIm labeling is absent. **J:** FluoroGold labeling of nuclei SpVm, PCRt, and IRt. The magnified and rotated image (box) shows neurons along the border between SpVi and SpVc.
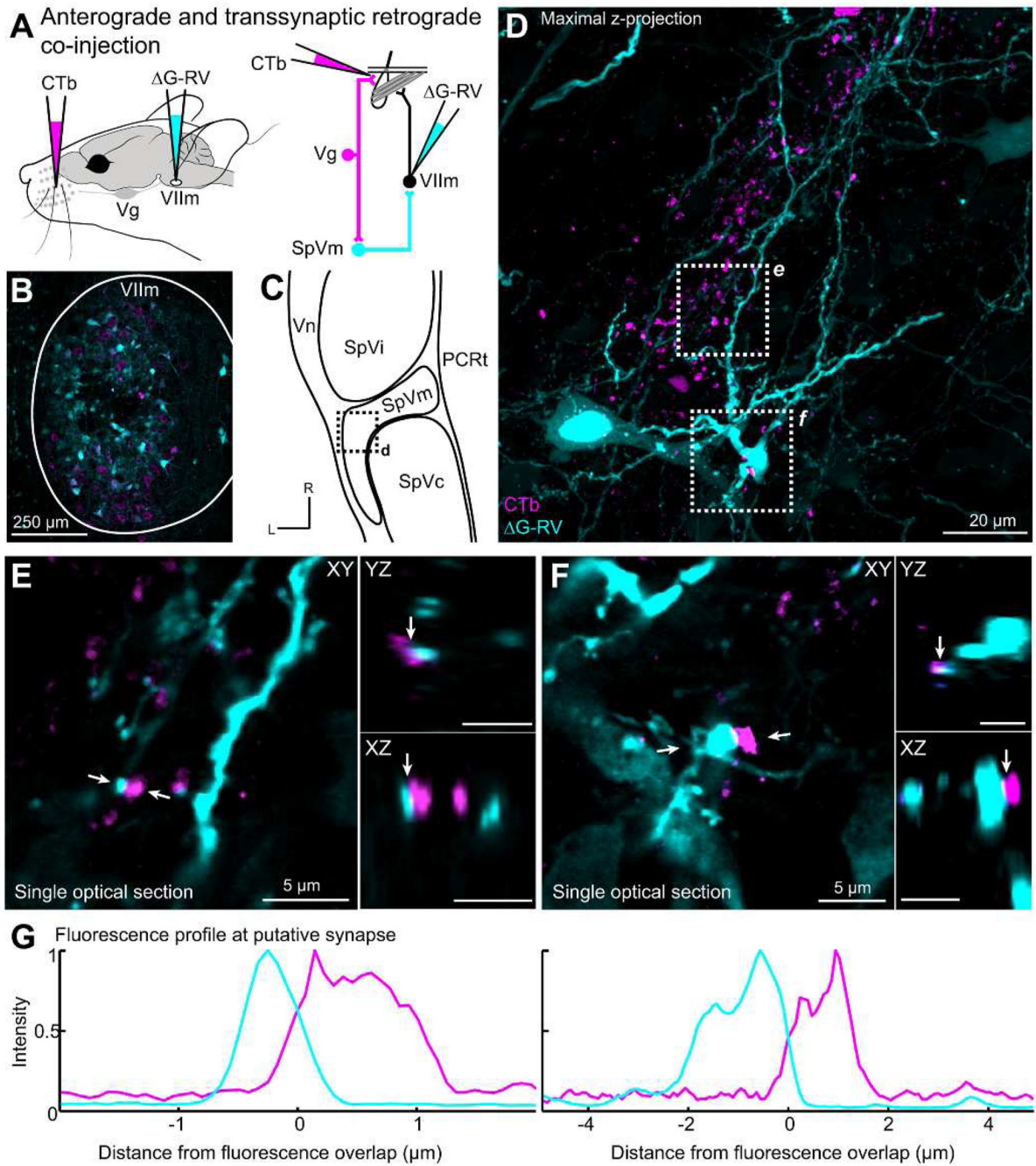
Figure 7. Dual labeling of primary afferent neurons and VIIm-projecting neurons in SpVm
A: Injection strategy. CTb was injected into the mystacial pad to label peripheral sensory afferent neurons, while ΔG-RV was injected into VIIm to label motoneurons. **B:** VIIm motoneurons were labeled in lateral VIIm (cyan). CTb (magenta) is also present as it travels both anterogradely and retrogradely from peripheral targets. We did not transect VII nerve, which would have prevented retrograde CTb labeling yet compromised VIIm motoneuron viability and, thus, rabies transduction. Spurious CTb labeling from VIIm is unexpected as there are no known axonal arbors of VIIm motoneurons that extend to non-muscle targets.

C: Anatomical organization of trigeminal nuclei for orientation and location of images in panels D to F. **D:** Maximal projection through 30 planes (15 μm, dorsoventral) showing SpVm. Dendritic trees of   G-RV-positive neurons (cyan) in SpVm are abundant, and peripheral axonal endings (CTb, magenta) terminate throughout SpVm. **E–F:** Representative putative synaptic contact examples (indicated with arrows) from d. A single plane is shown in each orthogonal slice, showing the apposition of CTb and   G-RV labels in SpVm. (g) Representative fluorescence profiles of putative synapses in a single XY plane taken from a ~ 300 nm (4 pixel) wide line between the arrows in e and f. Fluorescence intensity (ordinate axis) is normalized per channel. The distances between profiles at the half-maximum point of profile overlap are 290 (left) and 310 nm (right).
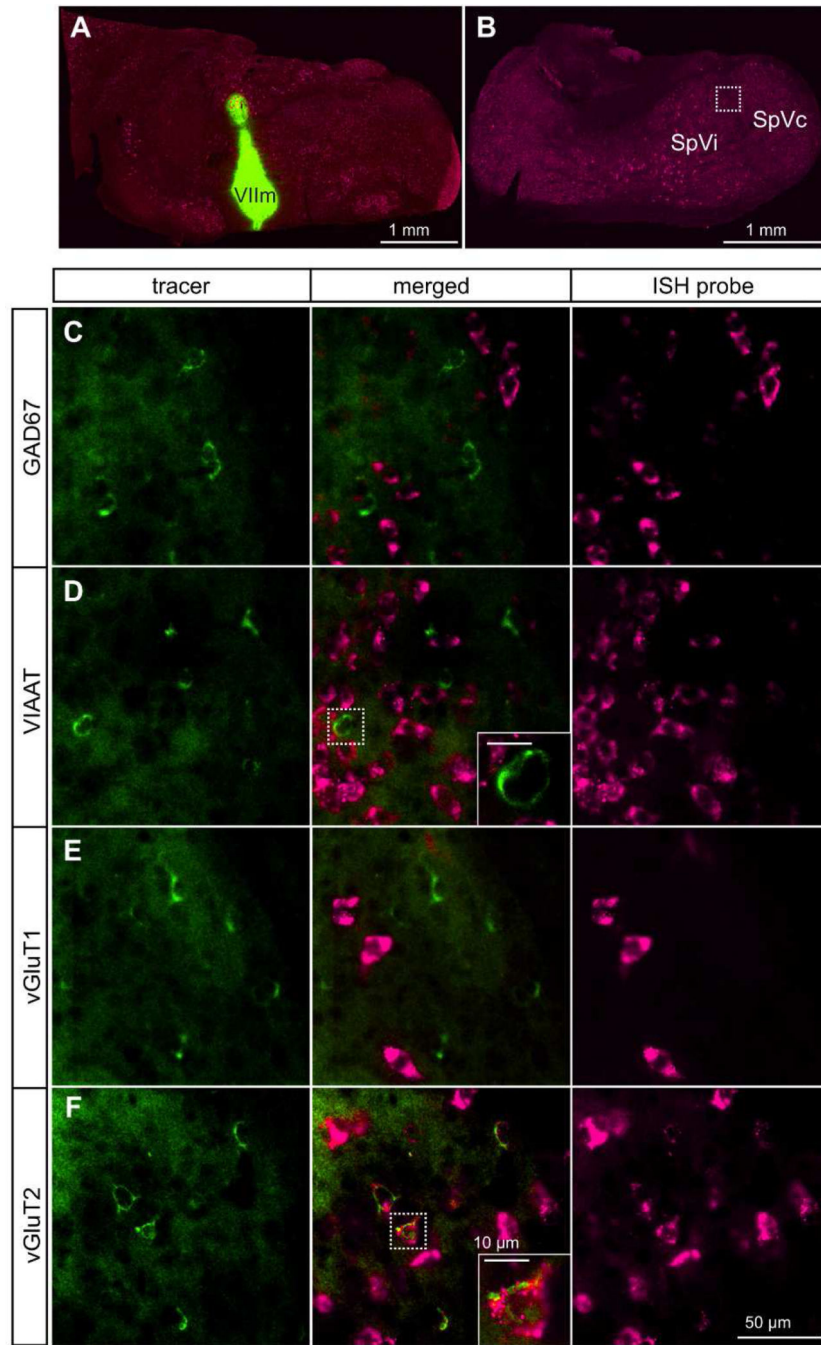
Figure 8. Neurotransmitter phenotype of SpVm neurons
A: Representative injection in VIIm of CTb (green) with a sample ISH probe (red) for contrast. **B:** Example location in SpVm for neuron counting (box). (c–d) Sample ISH of inhibitory neuron transcripts for g-aminobutyric acid (GAD67) (c) and vesicular inhibitory amino acid transporter (VIAAT) **D:** Inset in panel D to assess colocalization of tracer and probe (under 40× magnification confocal). **E–F:** Sample ISH of excitatory neuron transcripts for vesicular glutamate transporter 1 (vGluT1; panel E) and vesicular glutamate

transporter 2 (vGluT2; panel F). Inset in panel F to assess colocalization of tracer and probe, scale bar 10 μm (under 40× magnification confocal).
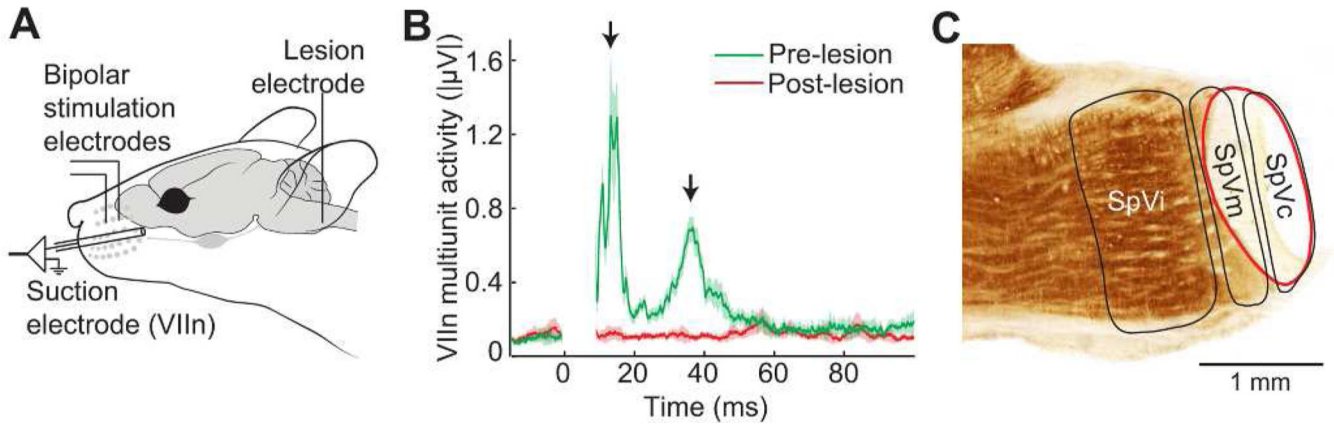
Figure 9. SpVm is necessary for vibrissa reflex circuit activity
A: Experimental ketamine-anesthetized setup. A bipolar electrode is positioned for mystacial pad stimulation to displace vibrissae, and activity from the transected buccal branch of the facial nerve is recorded with a suction electrode. Electrolytic lesion is performed in SpVm. **B:** VIIn multiunit activity in response to electrical stimulation of mystacial pad (mean ± 0.95 C.I.). Electrical activity is filtered and rectified (see Methods). VIIn has two peaks in activity following sensory stimulation, both of which are eliminated following lesion of SpVm. **C:** Representative histological slices confirming the lesion locations. The total current density and number of lesion locations was constant across experiments.
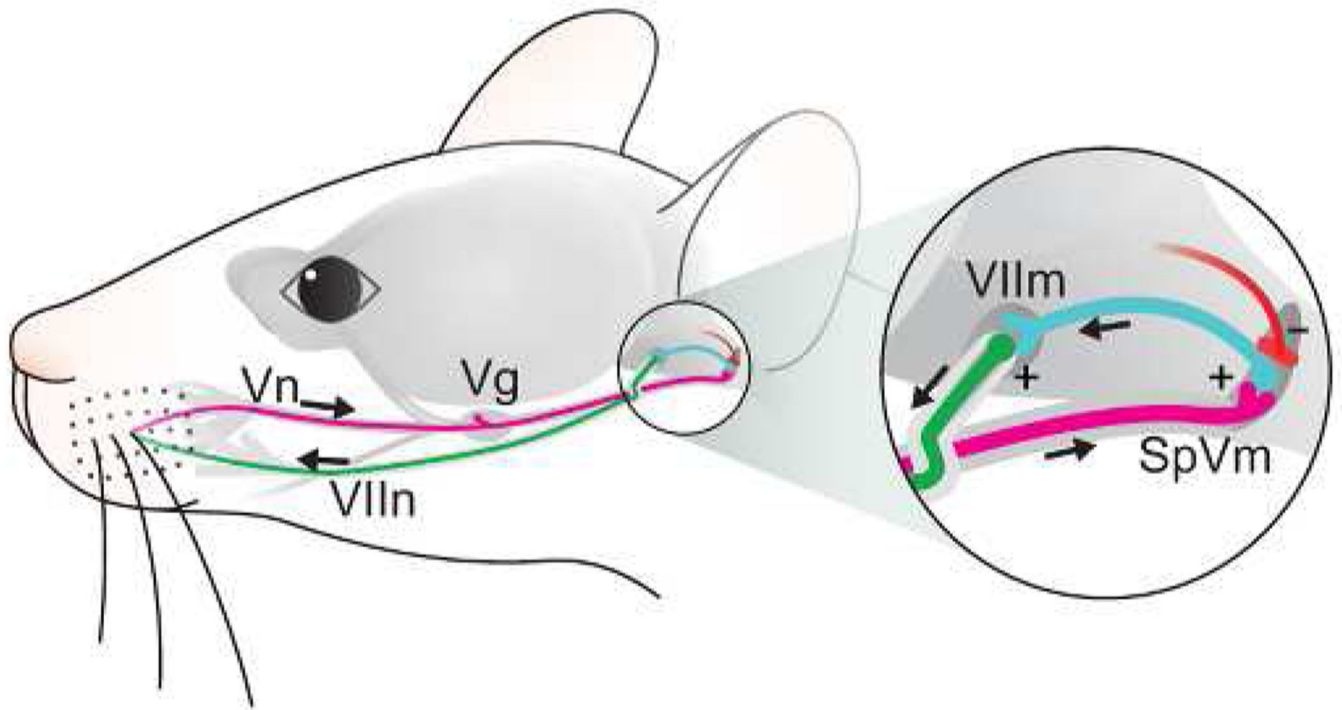
Figure 10. Summary of the circuit
Sensory axons (purple) terminate on neurons in SpVm (cyan), which can be modulated by feedforward or top-down inhibition (red) and project to VIIm motoneurons (green) responsible for whisking.

Table 1

In situ hybridzation (ISH) markers

GAD67	Description	Glutamic acid decarboxylase catalyzes decarboxylation of glutamate to GABA and CO_2.
	Marks	GABA-ergic neurons
	cDNA	Nucelotides 276–894
	GenBank	Accession number NM_008077
	Sequence	ggagc ggatcctaat actaccaacc tgcgccctac aacgtatgat acttggtgtg gcgtagccca tggatgcacc agaaaactgg gcctgaagat ctgtggcttc ttacaaagga ccaatagcct ggaagagaag agtcgtcttg tgagcgcctt cagggagagg cagtcctcca agaacctgct ttcctgtgaa aacagtgacc agggtgcccg cttccggcgc acagagaccg acttctccaa cctgtttgct caagatctgc ttccagctaa gaacggggag gagcaaactg cgcagttctt gctggaagtg gtagacatac tcctcaacta tgtccgcaag acatttgatc gctccaccaa ggttctggat ttccaccacc cacaccagtt gctggaaggc atggaaggct ttaatttgga gctgtctgac caccccgagt ctctggagca gatcctggtt gactgtagag acaccctgaa gtacggggtt cgcacaggtc accctcgatt tttcaaccag ctctctactg gtttggatat cattggttta gctggtgaat ggctgacatc gactgccaat accaatatgt tcacatatga aattgcaccc gtgt
VIATT	Description	Vesicular inhibitory amino acid transporter
	Marks	GABA-ergic and Glycine-ergic neurons
	cDNA	Nucelotides 866 –1817
	GenBank	Accession number NM_008077
	Sequence	gccat tcagggcatg ttcgtgctgg gcctacccta cgccatcctc cacggcggct acctgggggtt gttcctcatc atcttcgccg cagtggtgtg ctgctacacc ggcaagatcc tcatcgcgtg cctgtacgag gagaacgaag acggggaggt ggtgcgcgtg cgggactcgt atgtggccat agctaacgca tgctgcgctc ctcgattccc caccctgggc ggccgcgtgg tcaatgtggc gcagatcatc gagctggtga tgacgtgtat cttgtacgtc gtggtgagcg gcaacctcat gtacaacagt ttccccggggc tgcccgtgtc gcagaagtcc tggtccatca tagccacagc ggtgctgctg ccctgcgcct tcctgaagaa tctcaaggcc gtgtccaagt tcagtctgct gtgtacgctg gcccacttcg tcatcaacat cctggtcatc gcttactgtc tctctcgcgc gcgtgattgg gcctgggaga aggtgaagtt ctacatcgac gtcaagaagt ttcccatctc cattggcatc atcgtgttca gctacacgtc gcagatcttc ctgccctctc tcgaaggcaa catgcagcag cccagcgaat tccactgcat gatgaactgg acacacatcg ccgcctgcgt gctcaagggt ctcttcgcgc tcgtcgccta cctcacctgg gccgacgaga ccaaggaagt catcacggat aacctgcccg gctccatccg cgccgtggtc aacctcttcc tggttggccaa ggcgctgctg tcctatccgt tgcccttctt cgccggccgtc gaagtgctgg agaagttctct cttccaggaa ggcagtcgcg ccttcttccc cgcctgctat ggaggcgacg gtcgccttaa gtcctggggg ctgacgctgc gctgcgcgct ggtggtcttc acgctgc
VGluT1	Description	Vesicular glutamate transporter type 1
	Marks	Excitatory neurons
	cDNA	Nucelotides 855–1788
	GenBank	Accession number XM_133432.2
	Sequence	gcacag ccaccatgga gttccggcag gaggagtttc ggaagctggc ggggcgcgcc ctggggaggc tgcaccggtt actggagaag cggcaggaag gcgcggagac actggagctg agtgccgacg ggcggccagt gaccacgcac actcgggacc cgcctgtggt ggactgcacc tgctttggcc tccctcgtcg ctacatcatc gccatcatga gcggtctggg tttctgtatc agctttggca tccgctgcaa cctgggcgtg gccatcgtgt ccatggtcaa caacagcaca acccaccgtg ggggccacgt ggtggtgcag aaagcccagt tcaactggga tccagagact gtcggcctca tacatggctc ctttttctgg ggctacattg tcactcagat tcctgctggga tttatctgcc aaaaattcgc agccaacagg gtctttggct ttgccattgt ggctacctcc accctaaaca tgttgatccc ttcagcagcc cgccgttcact atggctgtgt catcttcgtg aggatcctcc agggattggt ggaggggggtc acatacctg cttgccatgg catctggagc aaatgggccc ctcccttaga acggagtcgg ctggcaacga cagcctttg cggttcctat gctgggggcgg tggttgccat gcccttggct ggggtccttg tgcagtattc aggatggagt tctgtcttct atgtctatgg cagcttcggg atcttttggt acctgttctg gttgcttgtc tcctatgagt caccggcact gcaacccagc atctctgagg aggagcgcaa atacattgag gatgccatcg gggagagcga caagctcatg aaccctgtta cgaagtttaa cacaccctgg aggcgcttct ttacgtgtcat gcccgtctat gccatcat
VGluT2	Description	Vesicular glutamate transporter type 2
	Marks	Excitatory neurons
	cDNA	Nucelotides 848–2044
	GenBank	Accession number NM_080853.2
	Sequence	cc atcgtggaca tggtcaacaa cagcactatc caccgcggag gcaaagttat caaggagaaa gccaaattta ctgggaccc cgagaccgtg gggatgatcc acggatcgtt cttctggggc tatatcatca cccagattcc aggaggatat atcgcatcgc ggctggctgc taaccgagtc tttggggctg cgatatgct cacctctacc ctcaatatgc tgatcccatc tgcagccaga gtgcattatg gatgtgtcat ctttgttagg atattgcaag gacttgtgga gggtgtcac taccagcct gtcatgggat atggagcaag tgggccctc ccttggagag gagtaggttg gctacaacct cctttgtgg ttcctatgct ggagcagtca ttgcaatgcc cttagctggt atccttgtc agtacactg atggtcgtca gtattttatg tgtatggaag ctttggcatg gtctggtaca tgttctggct tctggtgtct tatgagagcc ctgcaaagca tcctaccatt acagatgaag aacgtaggta catagaggag agcattggag agagcgcaaa tctgctaggt gcaatggaaa aatttaagac cccatgggag aagtttttca catcatgcc cgtctacgcg ataattgttg ccaactctgg caggagctgg actttttatt tactgctcat cagtcagcca gcttattttg aggaggttt tggatttgaa atcagcaagg ttggcatgtt gtctgcagtc cctcacctig tcatgacaat cattgtgcct atcgggggggc aaattgcaga tttcctaagg agcaagcaaa ttctctcaac aactacagtg agaaagatca tgaattgtgc ggggttttggc atggaagcca cgctgcttct ggttgttggc tactctcata ctagaggggt ggccatctcc ttcttggtgc ttgcagtagg attcagtgga tttgctatct

		ctggtttcaa tgttaatcac ttggatattg ctccaagata tgccagtatc ttaatgggca tttcagatgg cgttggcacg ctgtcgggga tggtttgccc tatcattgtt ggtgcaatga caaagaataa gtcccgtgaa gaatggcagt atgtcttcct cattgctgca ctcgtccact atggtggagt cata